



**Codes And Methods Improvements
for VVER comprehensive safety assessment**

Grant Agreement Number: 945081

Start date: 01/09/2020 - Duration: 36 Months

WP6 - Task 6.1

**D6.1 – Description of CFD models from partners
Results of outlet flow distribution benchmark**

Olivier Bernard (FRAMATOME)
Michael Böttcher (KIT)
Artur Hashymov, Denis Ruban (ENERGORISK)
Ulrich Bieder, Raksmy Nop (CEA)
Ossama Abdelhalim, Andrea Pucciarelli (UNIPI)

Version 1 – 18/02/2022



This project has received funding from the Euratom research and training programme 2019-2020 under grant agreement No 945081.

CAMIVVER – Grant Agreement Number: 945081

Document title	Description of CFD models from partners – Results of outlet flow distribution benchmark
Author(s)	Olivier Bernard (FRAMATOME), Michael Böttcher (KIT), Ulrich Bieder, Raksmy Nop (CEA), Ossama Abdelhalim, Andrea Pucciarelli (UNIPI), Artur Hashymov, Denis Ruban (ENERGORISK)
Document type	Deliverable
Work Package	WP6
Document number	D6.1 - version 1
Issued by	FRAMATOME
Date of completion	18/02/2022
Dissemination level	Public

Summary

CAMIVVER WP6 is dedicated to the CFD analysis of VVER-1000 vessel, and especially to the evaluation of flow mixing in the bottom part of the vessel.

This report describes the achievements of task 6.1:

- Preparation of a common CAD model of VVER vessel to be used for WP6.
- Preparation of CFD models from each WP6 partners. These CFD models are described in this report.
- Check of CFD models consistency on a nominal full-power steady-state benchmark.

Although CFD models have been developed by several participants (KIT, FRAMATOME, CEA, UNIPI, ENERGORISK) using different CFD tools (CFX, FLUENT, STAR-CCM+, TRIO-CFD), these models have provided consistent results in term of core-outlet temperature distribution.

These CFD models are now to be used within task 6.2 dedicated to Kozloduy-6 mixing experiment exercise.

Approval

Version	First Author	WP leader	Project Coordinator
1	O. BERNARD (FRAMATOME) 18/02/2022	O. BERNARD (FRAMATOME) 18/02/2022	D. VERRIER (FRAMATOME) 18/02/2022
	Signature 1 st author 	Signature WP leader 	Signature Coordinator 

Table of contents

Summary	2
INTRODUCTION	6
1. Illustration of common CAD model	7
2. Description of reference nominal full-power parameters for CFD models	9
3. Description of UNIPI STAR-CCM+ model	10
3.1. Introduction	10
3.2. Numerical models and nodalizations	10
3.3. Boundary conditions	12
3.4. Results and discussion	14
3.5. Conclusions.....	16
4. Description of CEA TRIO-CFD model	17
4.1. The CAD model.....	17
4.2. Meshing of the Flow Domain	18
4.3. The TrioCFD code.....	19
4.4. Conservation Equations	19
4.5. Discretization.....	20
4.6. Solution Method	21
4.7. Modelling of the core region	21
5. Description of KIT CFX model	24
6. Description of FRAMATOME STAR-CCM+ model	28
6.1. Geometry	28
6.2. Meshing.....	28
6.3. Boundary conditions	29
6.4. Head loss coefficients.....	29
6.5. Power source	30
6.6. Numerical parameters	31
7. Description of ENERGORISK Fluent model	32
7.1. General approach to RPV modelling	32
7.2. Geometry and mesh model	34
8. Nominal full-power steady-state results	38
8.1. Fuel Assemblies numbering	38
8.2. Fuel power profile.....	38
8.3. Outlet massflow profile	39
8.4. Outlet temperature profile.....	39
9. Conclusion	41
REFERENCES	42

List of Figures

FIGURE 1.1: CAD MODEL OVERVIEW (CORE IN ORANGE, CORE BASKET IN DARK)	7
FIGURE 1.2: CAD MODEL OVERVIEW (VESSEL ON THE LEFT, FUEL ASSEMBLY ON THE RIGHT)	7
FIGURE 1.3: CAD MODEL OVERVIEW (INNER VESSEL BOTTOM).....	8
FIGURE 2.1: ILLUSTRATION OF RADIAL POWER MAP (LEFT) AND AXIAL POWER MAP (RIGHT)	9
FIGURE 3.1: GEOMETRY OF THE VVER-1000 RPV AND PRESSURE MEASUREMENT POINTS.	10
FIGURE 3.2: CROSS SECTIONAL VIEW OF THE FLUID DOMAIN.	12
FIGURE 3.3: CROSS SECTIONAL VIEW OF THE MESHED DOMAIN: LOWER PLENUM (LEFT), UPPER PLENUM (RIGHT).	12
FIGURE 3.4: THE FULL MESHED CORE MODEL.	13
FIGURE 3.5: RADIAL AND AXIAL POWER DISTRIBUTION MAPS FOR BOL OF THE 6TH FUEL CYCLE.....	14
FIGURE 3.6: VELOCITY FIELD DISTRIBUTION ALONG THE REACTOR PRESSURE VESSEL.	15
FIGURE 3.7: TEMPERATURE FIELD DISTRIBUTION: TOP OF ASSEMBLY (LEFT), INTERFACE OF UPPER CORE SUPPORT PLATE/UPPER PLENUM (RIGHT).	16
FIGURE 3.8: MASS FLOW PER ASSEMBLY (LEFT), AVERAGE TEMPERATURE PER TOP/"END OF HEATED SECTION" OF ASSEMBLY (RIGHT).	16
FIGURE 4.1 : CAD MODEL OF THE VVER INTERNALS (A), ZOOM TO THE UPPER PLENUM (B), ZOOM TO THE LOWER PLENUM (C).....	18
FIGURE 4.2: MESHING OF THE LOWER PLENUM OF THE VVER-1000 REACTOR	19
FIGURE 4.3 : VELOCITY (A) AND TEMPERATURE (B) IN A VERTICAL CUT PLANE FOR STABILIZED CONDITIONS.	22
FIGURE 4.4 : CONCENTRATION OF A PASSIVE SCALAR (A) AND TEMPERATURE AT THE END OF THE ACTIVE CORE (B).....	23
FIGURE 5.1: THE OLD (LEFT) AND NEW MODEL VERSION (RIGHT)	24
FIGURE 5.2: COARSE MESH (V1) AND VERY FINE MESH (V3)	25
FIGURE 5.3: FLOW THROUGH ELLIPTICAL BOTTOM PLATE HOLES BY USING DIFFERENT MESHES.....	25
FIGURE 5.4: TEMPERATURE DISTRIBUTION AT CORE OUTLET.....	26
FIGURE 5.5: MASS FLOW DISTRIBUTION AT CORE OUTLET	26
FIGURE 5.6: CORE OUTLET TEMPERATURE OF V3 AND CORRESPONDING ASSEMBLY POWER FACTORS BY TRACE/PARCS.....	27
FIGURE 6.1: OVERVIEW OF THE GEOMETRY.....	28
FIGURE 6.2: MESH OVERVIEW	29
FIGURE 6.3: RADIAL DISTRIBUTION OF POWER IN THE CORE	31
FIGURE 8.1: ILLUSTRATION OF ASSEMBLY NUMBERING	38
FIGURE 8.2: FUEL POWER MAP.....	38
FIGURE 8.3: ASSEMBLIES-OUTLET MASSFLOW MAP (ASSEMBLIES LOCATED AT THE PERIPHERY OF THE CORE ARE IDENTIFIED WITH A DARK MARK BELOW)	39
FIGURE 8.4: OUTLET TEMPERATURE MAP.....	40
FIGURE 8.5: OUTLET TEMPERATURE: DEVIATION TO PARTICIPANTS AVERAGE.....	40

List of Tables

TABLE 2-1: COMMON REFERENCE PARAMETERS FOR NOMINAL STEADY-STATE BENCHMARK	9
TABLE 3-1: IMPOSED BOUNDARY CONDITIONS	13
TABLE 3-2: COMPARISON OF PRESSURE LOSSES	14
TABLE 4-1: PARAMETERS FOR THE PRESSURE LOSS CORRELATION	21
TABLE 6-1: HEAD LOSSES IN THE VESSEL	30

Abbreviations

BOC	Beginning of cycle
CFD	Computational Fluid Mechanics
NPP	Nuclear power plant
RPV	Reactor pressure vessel

INTRODUCTION

CAMIVVER WP6 has the objective to improve CFD modelling and validation for VVER applications, especially mixing in primary vessel. In particular:

- Perform enhanced and updated CFD validation on Kozloduy-6 mixing experiment. Benchmark CFD analysis from partners regarding this experiment. This implies CFD models development and upgrades from partners.
- Proceed to uncertainty propagation through CFD models.

Task 6.1 is a preliminary task dedicated to the preparation of this work package, through the following stages:

- Preparation of a common CAD model of VVER vessel to be used for WP6. Paragraph 1 illustrates this CAD model.
- Preparation of CFD models from each WP6 partners. These CFD models are described from paragraphs 3 to 6.
- Check of CFD models consistency on a nominal full-power steady-state benchmark. The input data to be used for this benchmark are detailed in paragraph 2, and the results of the benchmark are described on paragraph 8.

1. Illustration of common CAD model

The common VVER vessel CAD model developed in the frame of WP6 is illustrated on Figure 1.1, Figure 1.2 and Figure 1.3. This CAD model is based on drawings available in CAMIVVER deliverable D3.1 [2].

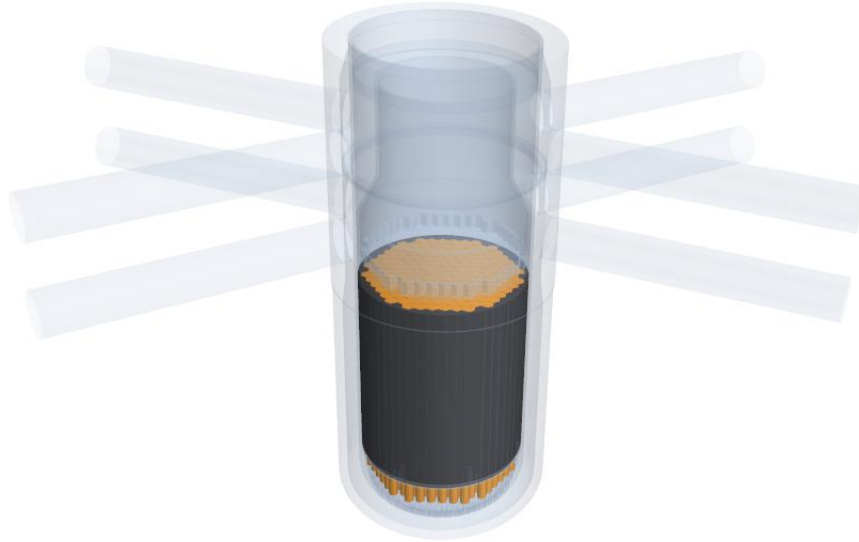


Figure 1.1: CAD model overview (core in orange, core basket in dark)

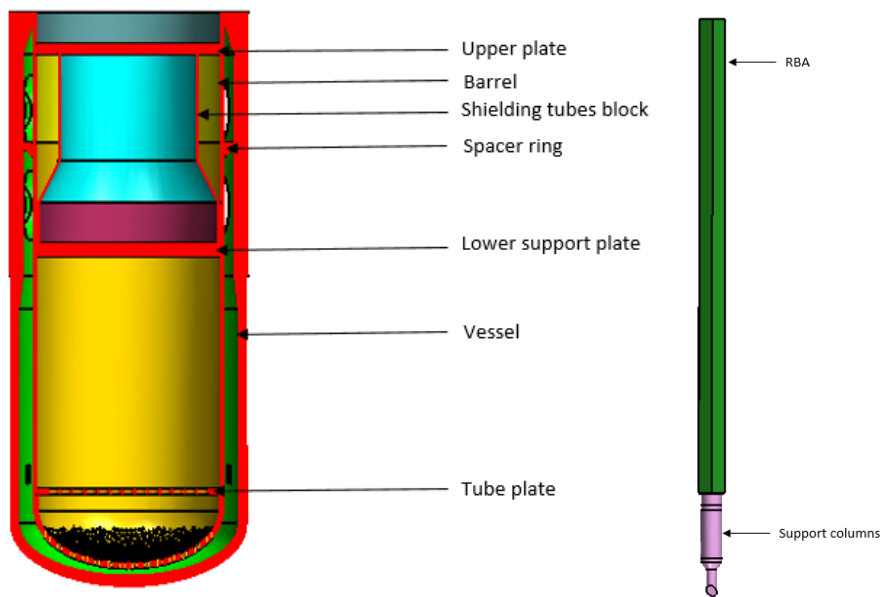


Figure 1.2: CAD model overview (vessel on the left, fuel assembly on the right)

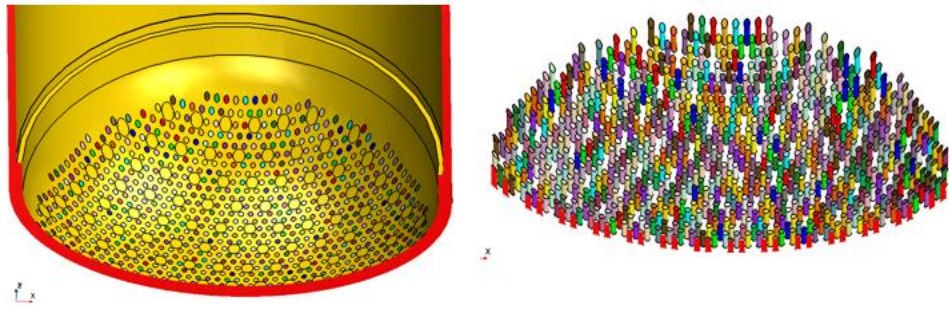


Figure 1.3: CAD model overview (inner vessel bottom)

2. Description of reference nominal full-power parameters for CFD models

The following parameters have been arbitrary selected for CFD models set-up and comparison:

Table 2-1: Common reference parameters for nominal steady-state benchmark

Parameters	Value	Comments
Vessel inlet temperature	287 °C 560,15 K	Temperature for incoming water through cold leg nozzles
CFD vessel flowrate	17434 kg/s	The total vessel flowrate is 17610 kg/s, but 1% of this flowrate is supposed to bypass the vessel by leaking from cold to hot leg. Therefore, the vessel flowrate is reduced to 17434 kg/s in CFD models
Core flowrate	16912 kg/s	The core-bypass flowrate is supposed to be 3% of the total CFD vessel flowrate.
Core-bypass flowrate	523 kg/s	
Core Power	3000 MW	
Power distribution	Table 3.3.1 of D3.2 Figure 3.3.2 of D3.2	The fuel loading is supposed to be <i>beginning of cycle 6, unit 6 of Kozloduy</i> . This fuel loading is described in CAMIVVER deliverable 3.2 [3], table 3.3.1 (begin of life) for the axial distribution and figure 3.3.2 for the radial distribution

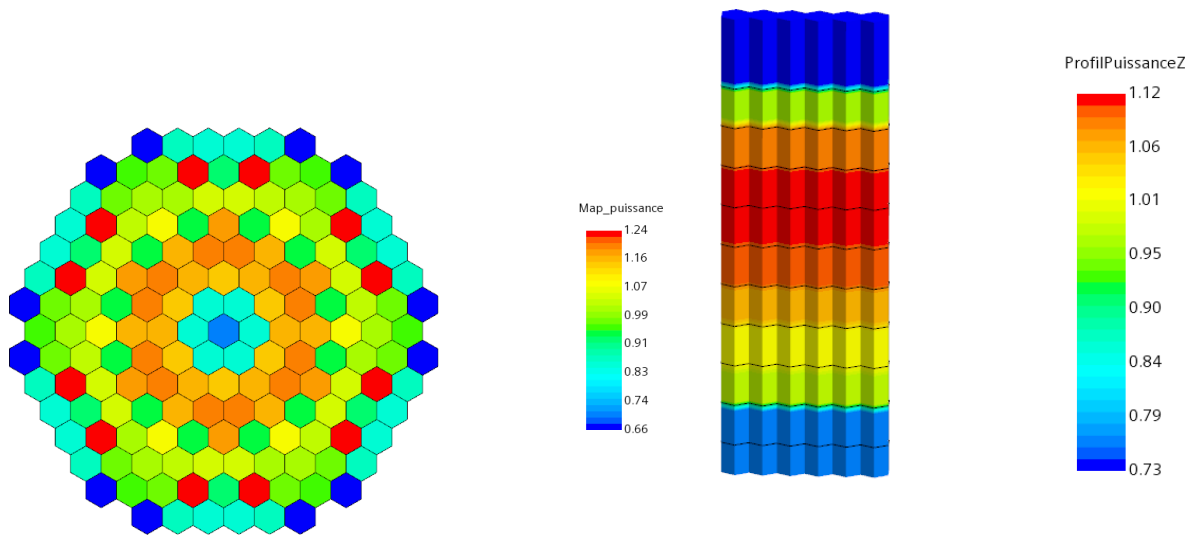


Figure 2.1: illustration of radial power map (left) and axial power map (right)

3. Description of UNIPI STAR-CCM+ model

3.1. Introduction

In the framework of the Codes And Methods Improvements for VVER comprehensive safety assessment project (CAMIVVER), a three-dimensional CFD model is developed for an improved description of the coolant mixing phenomena within the VVER reactor pressure vessel (RPV). The standard design of the VVER-1000 model V320 is considered; the reference data are derived from the operational data of the Kozloduy Unit 6 nuclear power plant (NPP) provided in work package 3 (WP3) report [3].

The VVER-1000/V320 is a pressurized water reactor of 3000 MW thermal power with four primary loops which produces 1000 MW of electric power. The nominal operating conditions of full power are 15.75 MPa of system pressure, 287°C of core inlet temperature and 17611 kg/sec of reactor coolant mass flow rate. The RPV has four inlet nozzles and four outlet nozzles to connect the primary loops and the primary sides of horizontal steam generators. The core is comprised of 163 hexagonal fuel assemblies (FAs) without a shroud (i.e., open type core); each FA contains 312 fuel pins, where the total active core height is 3550 mm starting 355 mm above the bottom of the FA.

The primary coolant enters from the inlet nozzles and mainly flows towards the downcomer; about 1% of the flow, instead, bypasses the core and directly reaches the hot leg through a spacer ring. After the downcomer, the flow reaches the elliptical bottom of the RPV, and it enters the perforated elliptical bottom of the core barrel which serves as distributor plate (see Figure 3.1). As soon as the coolant passes through the perforated elliptical bottom of the barrel, the coolant flows upward through the fuel supporting columns and into the bottom of FAs. The heads of the FAs connect the core flow to the upper plenum, where the flow exits to the outlet nozzles passing through the perforated frame of the shielding tubes block and then through the perforated section in the barrel.

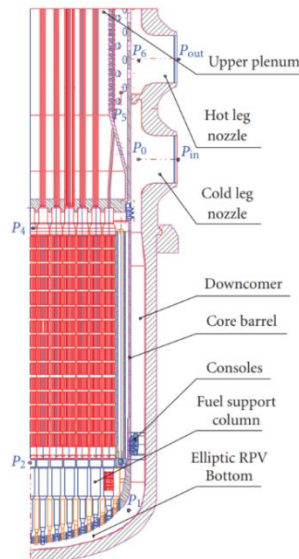


Figure 3.1: Geometry of the VVER-1000 RPV and pressure measurement points.

3.2. Numerical models and nodalizations

In order to simulate the involved phenomena, a full 3D geometry of the VVER-1000 was developed considering several geometrical simplifications to fit the computational capabilities and reduce the targeted computational cost. The developed geometry consists of inlet nozzles, downcomer, lower plenum, core region, upper plenum, and outlet nozzles. The spacer ring, which isolates the hot legs from the cold ones, was not modelled and, as a consequence, the bypass flow from hot to cold legs was taken into account while setting the boundary conditions: the imposed mass flow rate was thus

reduced by 1% with respect to the reference value. The core region was simplified to a hexagonal FA grid without modelling the fuel rods, spacer grids and inlet/outlet heads. Furthermore, the core basket was modelled as a hollow cylinder having a flat interface with the lower plenum to account for the core bypass as illustrated in Figure 3.2. The upper core support plate was modelled as a unique fluid region without any perforations preserving the continuity of core flow to the upper plenum. The upper plenum was assumed to be suitably modelled by a fluid region without including the shielding tube and control rod driving arms. Finally, the perforated frame of the shielding tube block and the perforated section of the barrel were modelled as fluid regions without any perforation. As a result of all these geometrical simplifications, only fluid regions were considered and no solid parts were modelled: the flow domain thus consists of the 7 fluid regions shown in Figure 3.2. Six porous regions were modelled due to the simplifications mentioned earlier, they are: core region, core basket, upper core plate, perforated frame of the shielding tubes block, the perforated barrel, and the upper plate. Thanks to the introduction of these porous media, the effects related to the fluid/solid interactions can be modelled by tuning the resistance parameters in the porous regions themselves: this allows for a smaller total element count and perpetuates the capability to reproduce the targeted pressure losses in Kozloduy Unit 6 NPP.

The modelled fluid region, which includes inlet/outlet nozzles, downcomer, lower and upper plena, was constructed by 24.8 million unstructured polyhedral cells. A cross sectional view of the lower and upper plena are shown in Figure 3.3. The modelled core region contains approximately 1 million cells, constructed from 50 prismatic cell layers generated from polygonal cells. Figure 3.4 shows the full meshed core region. Finally, all the porous regions were generated using unstructured polyhedral cells and constructed by 1.8 million cells. Therefore, the full geometry was constructed by a mesh grid of roughly 27.6 million cells. It is important to notice that, as emphasized earlier in this report, since neither the fuel pins in the FA nor the internal structure of the upper plenum was modelled, additional pressure losses were introduced in the porous regions in order to reproduce the design pressure losses measured at the positions P0, P2, P4, P5 and P6 as indicated on Figure 3.1, while operating at nominal conditions.

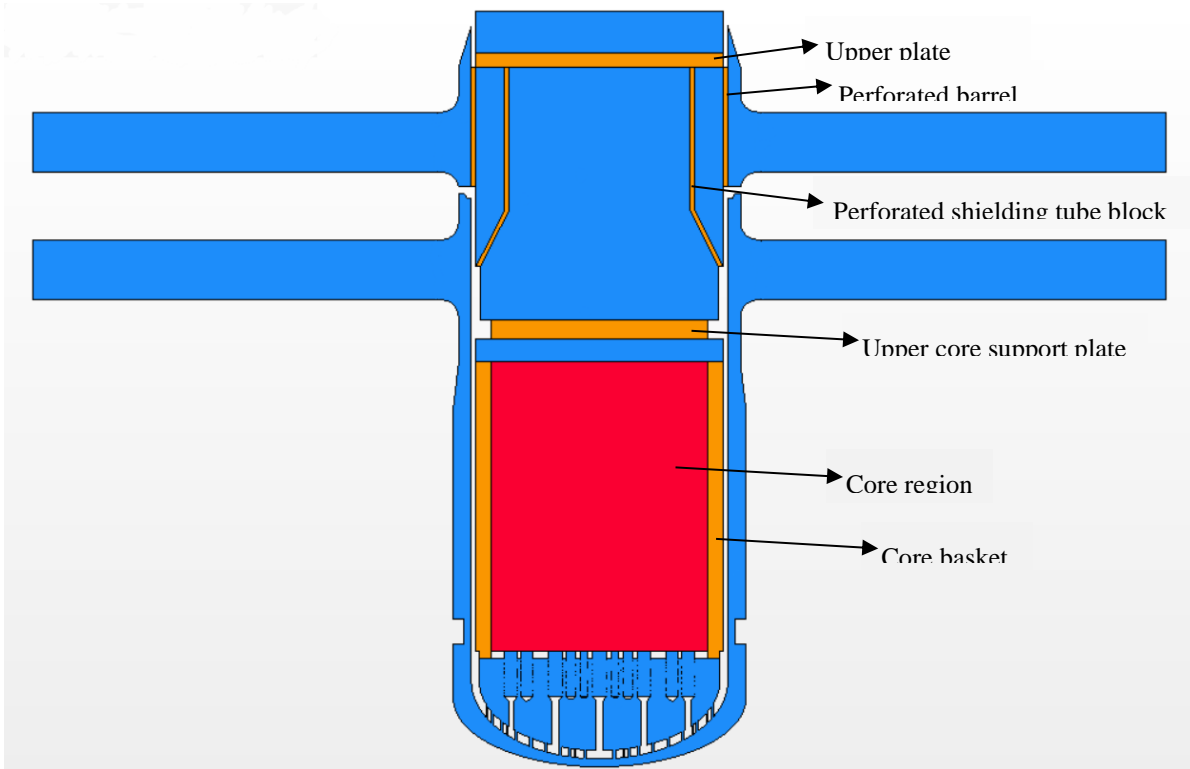


Figure 3.2: Cross sectional view of the fluid domain.

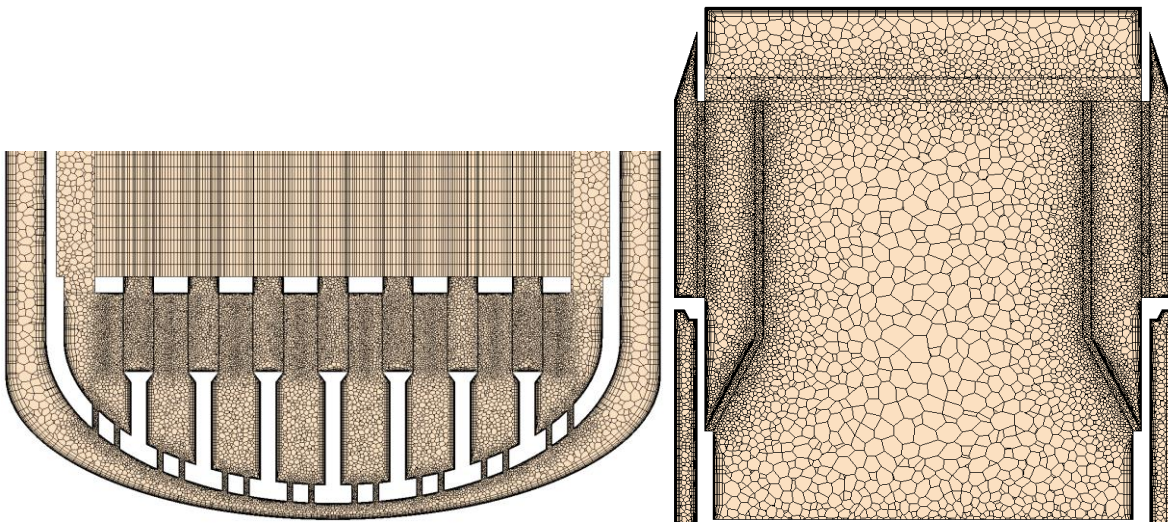


Figure 3.3: Cross sectional view of the meshed domain: lower plenum (left), upper plenum (right).

3.3. Boundary conditions

The developed numerical model is used to predict the VVER-1000 core outlet temperature and mass flow at the exit of the assemblies while operating at nominal conditions using the STAR-CCM+ code. The imposed boundary conditions are reported in Table 3-1. The properties of the coolant were introduced as temperature-dependent polynomials at a pressure of 15.5 MPa, assuming it to be close to the average pressure inside the core. The imposed 3000 MW thermal power in the active core region was considered assuming the axial power distribution for the average assembly and the

radial power distribution maps as shown in Figure 3.5 for Beginning Of Life (BOL) of the 6th fuel cycle of unit 6 of Kozloduy NPP as reported in WP3 report of A. Stefanova et al. [1].



Figure 3.4: The full meshed core model.

Table 3-1: Imposed Boundary conditions

Parameter	Value
Total core power output [MW _{th}]	3000
Core pressure [MPa]	15.75
Core inlet temperature [°C]	287
Total Mass flow rate* [kg/s]	17434.89
* - the value of the mass flow excluding the 1% cold-hot legs bypass	

The turbulence model adopted is a standard k-ε Low-Re model with all y+ wall treatment for near-wall flow with 2nd order convection scheme. In order to reproduce the pressure losses distribution for Kozloduy NPP, additional isotropic and orthotropic inertial porous resistance coefficients were used to set the pressure losses in the porous regions to match the pressure losses measured at the reference locations reported in Figure 3.1 for nominal steady-state conditions. A uniform azimuthal resistance coefficient of a value 26879 kg/m⁴ was used for the core region and no radial resistance was adopted for the core region. In addition, a uniform azimuthal resistance coefficient of a value 211202 kg/m⁴ was used for the core basket region, in order to predict a core-bypass mass flow rate close to the one estimated in the reference report [1], to be in the range of 3% of the total CFD vessel flowrate. Eventually, an overall isotropic resistance coefficient of a value 5900 kg/m⁴ was used for the upper plenum regions. These resistance coefficients are going to be maintained also for the transient computations foreseen for the next steps of the project. Table 3-2 presents a comparison between the measured pressure at reference locations and model CFD predictions for nominal steady state conditions.

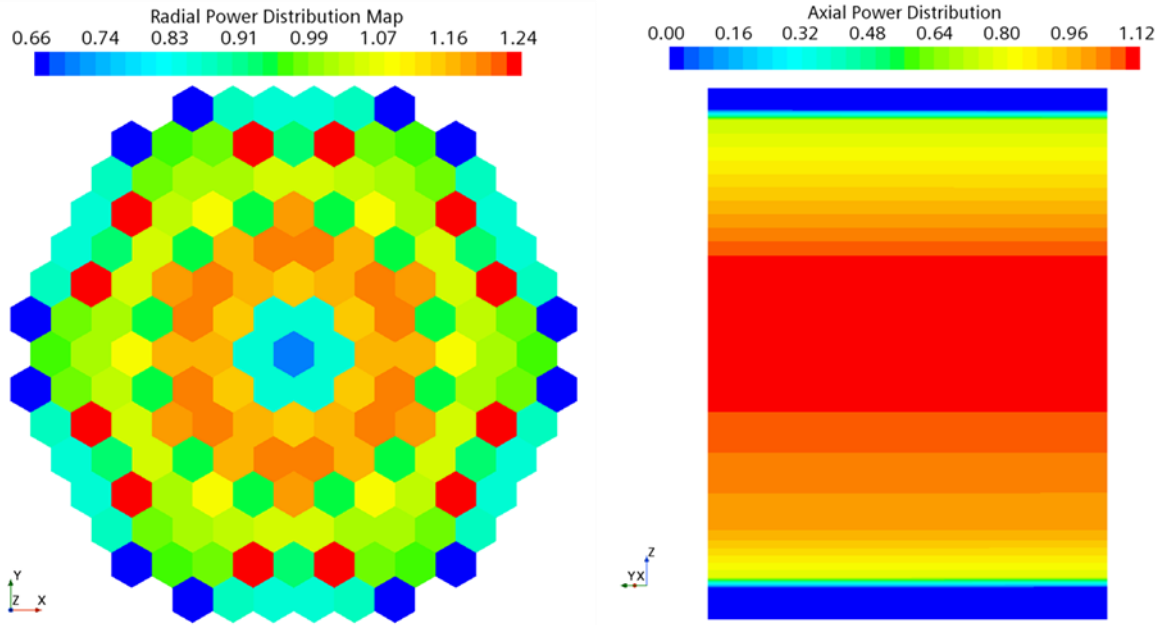


Figure 3.5: Radial and Axial power distribution maps for BOL of the 6th fuel cycle.

Table 3-2: Comparison of pressure losses.

ΔP	ΔP measured [MPa]	ΔP CFD [MPa]
P0 – P2	0.201	0.19551
P2 – P4	0.142	0.14199
P4 – P5	0.029	0.02897
P4 – P6	0.037	0.03689
P0 – P6	0.392	0.37141

3.4. Results and discussion

Figure 3.6 shows the velocity field distribution developed in the VVER-1000 reactor while operating at nominal steady-state condition. The velocity distribution in the downcomer is stable and a peak of the velocity magnitude is resolved in the vicinity of the inlet nozzles. The presence of the consoles, which hold the barrel in its position, slightly disturbs the flow entering the lower plenum. Starting from the consoles, the flow begins to accelerate up to reaching the centre of the bottom plate of the reactor vessel where it slows down, forming a sort of stagnation area. Then, the coolant enters the lower plenum via the perforated elliptical bottom plate of the barrel where the maximum of the velocity field is achieved.

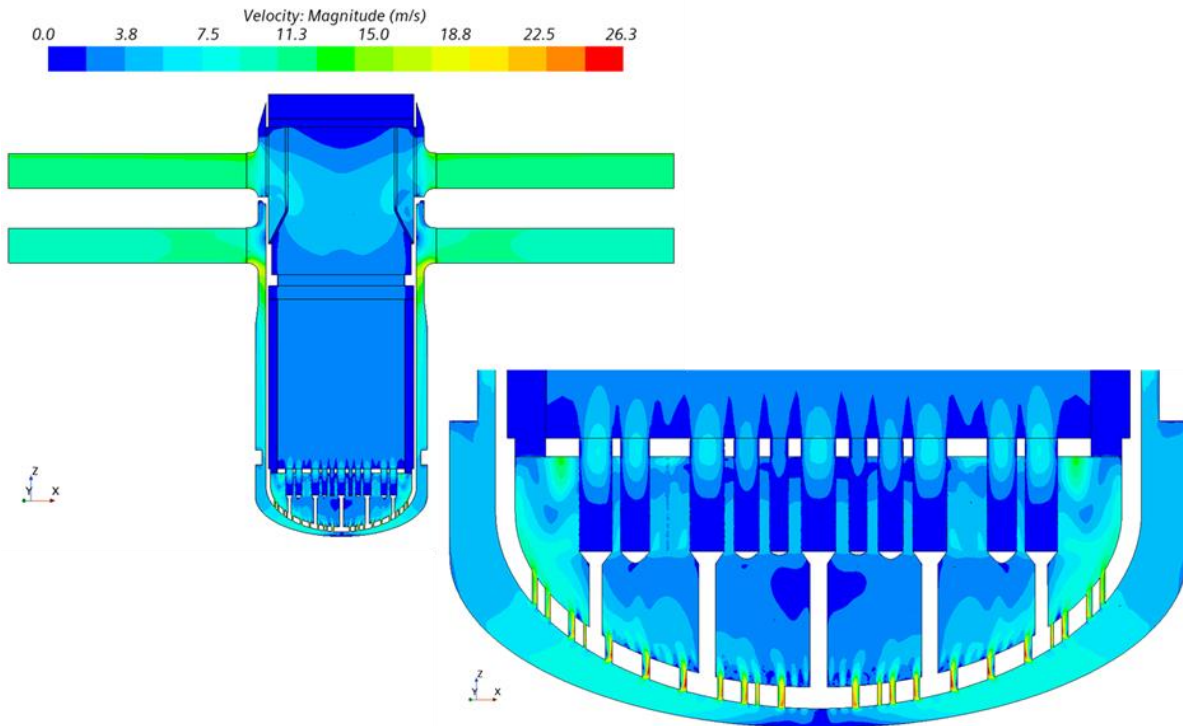


Figure 3.6: Velocity field distribution along the reactor pressure vessel.

The temperature distribution at the core outlet, shown in Figure 3.7, is coherent with the radial power distribution shown in Figure 3.5. Locations of the maximum temperature at top of assemblies (Figure 3.7 left) are following the peaks of the radial power factor as shown in Figure 3.5. On the other hand, the temperature field distribution just before entering the upper plenum (Figure 3.7 right) shows a wide dispersion for the maximum temperature, especially at the centre of the core with respect to its periphery, due to the mixing of the coolant after leaving the assemblies. Moreover, the average values of the computed temperature are in the same range of the measured data for nominal steady state operating conditions of Kozloduy-6 NPP.

Figure 3.8 shows the radial assembly-by-assembly mass flow and average temperature distributions. The computed assembly outlet temperatures refer to the end of the heated part of the assemblies and a good agreement is obtained compared to the measured data for nominal steady state. The average mass flow per assembly is 103.7 kg/s and the predicted mass flow is quasi symmetrical for all loops except for assembly no. 56, corresponding to loop no. 2, which shows a slightly lower mass flow rate compared to that central sector of the core. Also, the average temperature per top of assembly shown in (Figure 3.8 right) is quasi symmetrical for most of the core, except at the central part where assemblies no. 81 and no. 95 show a 1°C less compared to the rest of the central assembly ring.

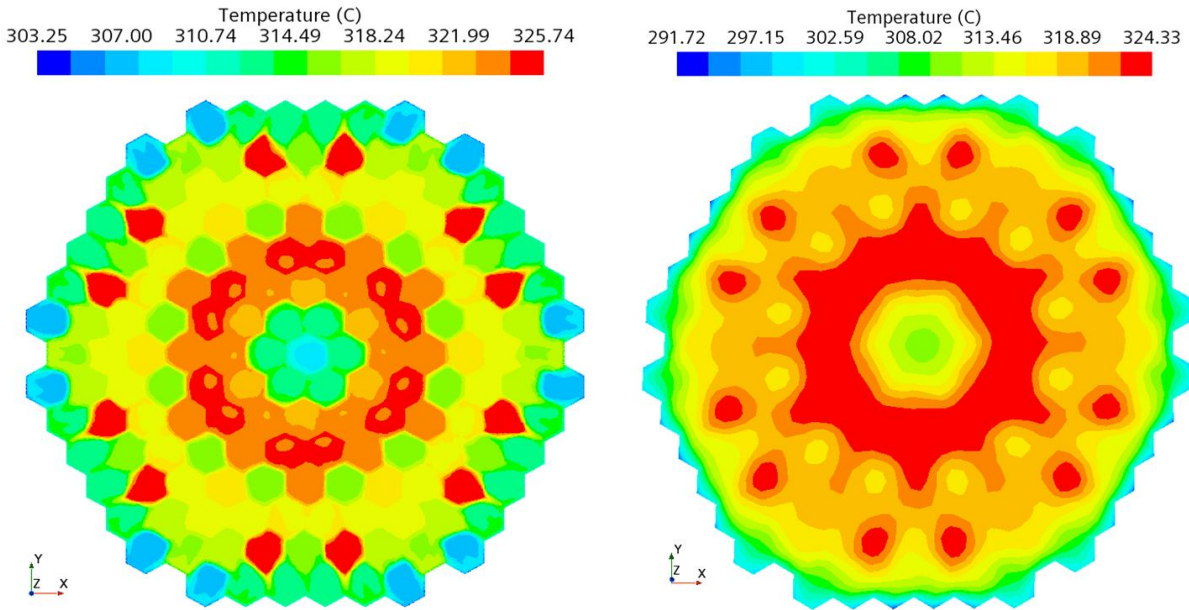


Figure 3.7: Temperature field distribution: top of assembly (left), interface of upper core support plate/upper plenum (right).

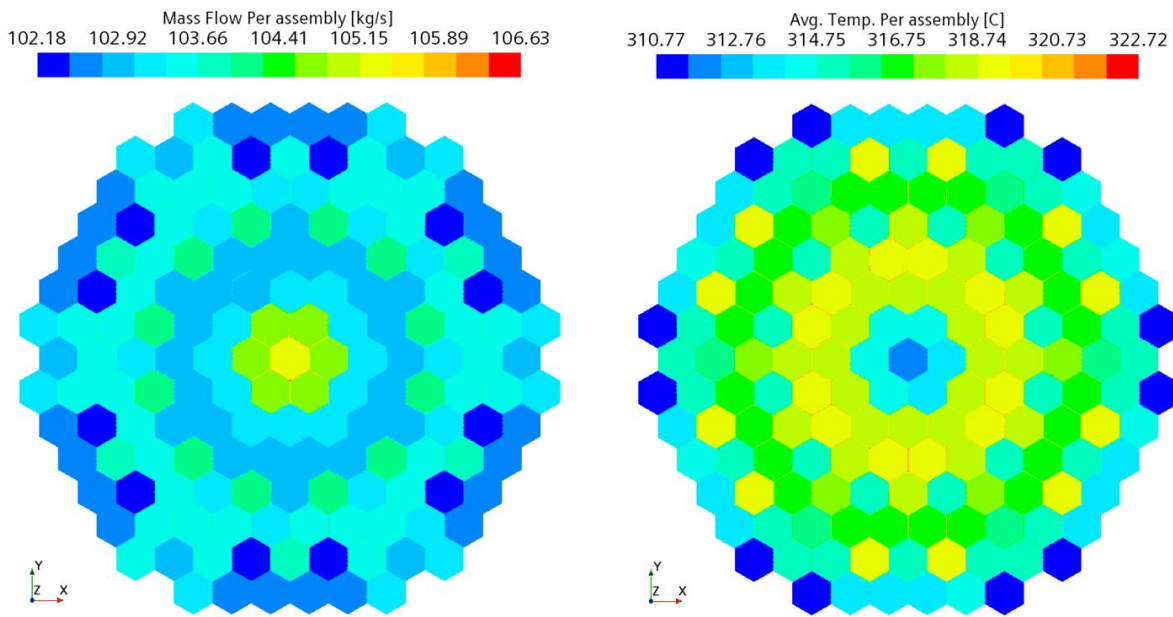


Figure 3.8: Mass flow per assembly (left), average temperature per top/end of heated section of assembly (right).

3.5. Conclusions

The analysis shows that the results are in good agreement in terms of pressure losses, average core outlet temperature and mass flow rate per assembly with respect to the measured data of Kozloduy-6 NPP. Such agreement was obtained under use of the actual nominal steady state boundary conditions and the choice of standard $k-\epsilon$ Low-Re model with all $y+$ wall treatment for near-wall flow. The CFD model was able to reproduce qualitatively well the flow and velocity distributions along the vessel and the accuracy of the CFD predicted temperature and mass flow needs to be estimated in order to draw a conclusion on the minor deviations in certain assemblies with respect to the entire core.

4. Description of CEA TRIO-CFD model

4.1. The CAD model

The VVER-1000 is a four loop pressurized water reactor with hexagonal fuel assemblies, horizontal steam generators and 3000 MW thermal power. The core is of open type and contains 163 fuel assemblies. Eight consoles centre the core barrel in the reactor pressure vessel (RPV). The simulated sections of the reactor start in the cold legs about 15 m upstream of the RPV inlet nozzles and end in the hot legs about 7.5 m downstream of the RPV outlet nozzles. Hot- and cold legs are taken as straight tubes, i.e. tube bends are neglected in the model. The coolant flows from the cold leg nozzles into the downcomer and further into the narrowing gap between RPV and elliptic core barrel bottom. The CAD model of the structures that are located inside the RPV is shown in Figure 4.1a (Feng and Bieder, 2016). The flow enters the lower plenum through the 1344 holes of the elliptic core barrel bottom. Then, the coolant passes into the fuel support columns, which serve as flow distributors. The slots of each mixing columns are modelled by four holes that respect the total cross-section of the slots. The primary coolant flows further upward through the core support plate into the fuel assemblies. These elements of the lower plenum are shown in more detail in Figure 4.1c. The flow leaves the core by flowing across the upper core plate and enters the upper plenum. The guide tubes are simplified in the CAD model as straight tubes. In the upper plenum, the flow passes the flow holes of the shielding drum as well as the flow holes of the upper core barrel before leaving the upper plenum by the hot leg nozzles. As shown in Figure 4.1c, these flow holes are taken into account explicitly in the model.

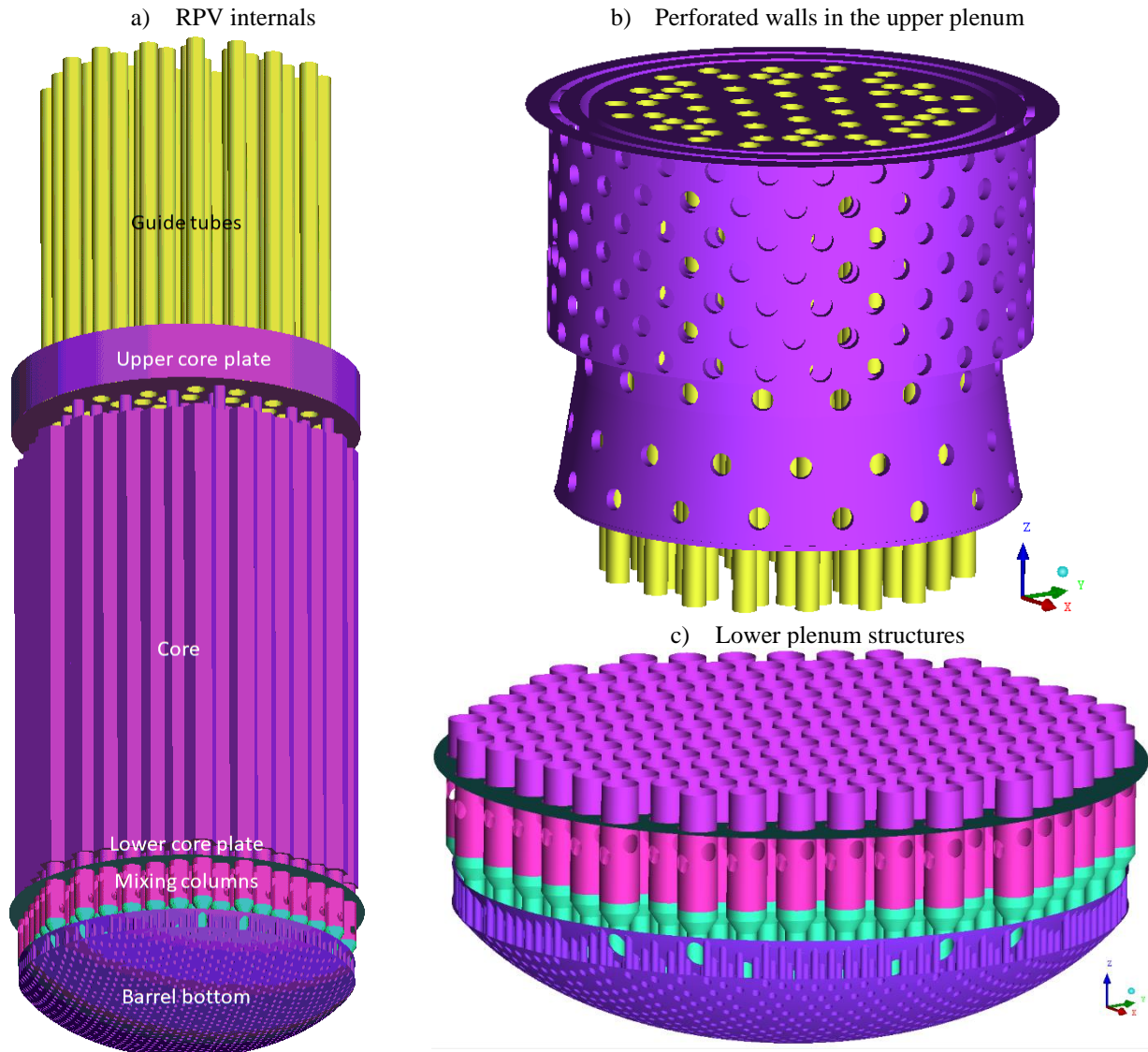


Figure 4.1 : CAD model of the VVER internals (a), zoom to the upper plenum (b), zoom to the lower plenum (c)

4.2. Meshing of the Flow Domain

From the described CAD model, a tetrahedral mesh of about 45 million elements has been created using the commercial mesh generator ANSYS-ICEMCFD (Feng and Bieder, 2016). A surface mesh was extracted from a preliminary tetrahedral mesh that has been produced by the OCTREE method. The final tetrahedral mesh was created by the DELAUNY method. Two prism layers were added at the downcomer walls. The dual-mesh discretization used in TrioCFD leads to about 90 million control volumes for each velocity component of the momentum equations. This reference mesh is shown in Figure 4.2 for the narrowing gap and lower plenum. For sensitivity tests, it is possible to further refine the mesh homogeneously by dividing each tetrahedral cell into 8 sub-tetrahedrons.

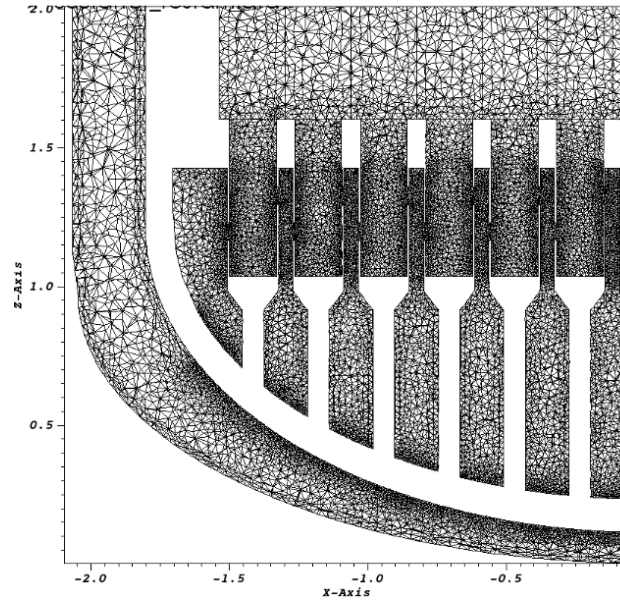


Figure 4.2: Meshing of the lower plenum of the VVER-1000 reactor

4.3. The TrioCFD code

TrioCFD (Angeli et al., 2018) is a general CFD code based on the TRUST platform (Saikali et al., 2021). The code is developed at CEA-Saclay and has been especially designed for turbulent flows in complex geometries. The platform independent code is based on an object oriented, intrinsically parallel approach and is coded in C++. The flexible code structure allows the user to choose a suitable discretization method and to combine various appropriate physical models. Several convection and time marching schemes as well as wide range of boundary conditions are available.

4.4. Conservation Equations

The Reynolds averaging procedure is applied on the instantaneous velocity u , which is decomposed into a statistical mean value \bar{u} and a fluctuating component u' . Using the Einstein notation, the mean velocity is determined by the equations of mass conservation (eq.(1)) and momentum conservation (eq.(2)) (Pope, 2000). Thermal effects are neglected in the momentum equations, as the local Reynolds numbers are very high. External forces are taken into account by the momentum source term $F_{m,i}$.

$$\frac{\partial \bar{u}_j}{\partial x_j} = 0 \quad , \quad (1)$$

$$\frac{\partial \bar{u}_i}{\partial t} + \frac{\partial (\bar{u}_i \bar{u}_j)}{\partial x_j} = - \frac{\partial \bar{p}}{\rho \partial x_i} + \frac{\partial}{\partial x_j} \left[\nu \left(\frac{\partial \bar{u}_i}{\partial x_j} + \frac{\partial \bar{u}_j}{\partial x_i} \right) - \bar{\tau}_{ij} \right] + F_{m,i} \quad , \quad (2)$$

Applying the Boussinesq hypothesis, the Reynolds stress tensor τ_{ij} is defined according to eq.(3):

$$\bar{\tau}_{ij} \equiv -\overline{u'_i u'_j} = \nu_t \left(\frac{\partial \bar{u}_i}{\partial x_j} + \frac{\partial \bar{u}_j}{\partial x_i} \right) - \frac{2}{3\rho} k \delta_{ij} \quad (3)$$

Eq.(4) describes the conservation of energy.

$$\frac{\partial \bar{T}}{\partial t} + \bar{u}_j \frac{\partial \bar{T}}{\partial x_j} = \frac{\partial}{\partial x_j} \left[\left(\frac{\lambda}{\rho c_p} + \frac{\lambda_t}{\rho c_p} \right) \frac{\partial \bar{T}}{\partial x_j} \right] + F_e \quad . \quad (4)$$

The following formulation of the k-ε model is used (Pope, 2000) to evaluate the turbulent viscosity ν_t :

$$\frac{\partial k}{\partial t} + \frac{\partial(\overline{u_j k})}{\partial x_j} = \frac{\partial}{\partial x_j} \left[\left(\frac{\mu}{\rho} + \frac{\mu_t}{\rho \cdot \sigma_k} \right) \frac{\partial k}{\partial x_j} \right] - \varepsilon + P \quad , \quad (5)$$

$$\frac{\partial \varepsilon}{\partial t} + \frac{\partial(\overline{u_j \varepsilon})}{\partial x_j} = \frac{\partial}{\partial x_j} \left[\left(\frac{\mu}{\rho} + \frac{\mu_t}{\rho \cdot \sigma_\varepsilon} \right) \frac{\partial \varepsilon}{\partial x_j} \right] + C_{\varepsilon 1} P \frac{\varepsilon}{k} - C_{\varepsilon 2} \frac{\varepsilon^2}{k} \quad (6)$$

$$\text{with } \nu_t = c_\mu \frac{k^2}{\varepsilon} \quad \text{and} \quad P = -\overline{u'_i u'_j} \frac{\partial \overline{u_i}}{\partial x_j}$$

The Reynolds stresses $\overline{u'_i u'_j}$ in the production term P are calculated from eq.(3). The following empirical coefficients are used: $c_\mu = 0.09$, $\sigma_k = 1$, $\sigma_\varepsilon = 1.3$, $C_{\varepsilon 1} = 1.44$ and $C_{\varepsilon 2} = 1.92$.

At inflow faces, Dirichlet boundary conditions with imposed velocity are used. In this context, k and ε were calculated from a spatial mean velocity $|U_m|$ and a hydraulic diameter d_h , assuming a turbulence level of 10 % ($u' = 0.1 \cdot |U_m|$):

$$k = \frac{1}{2} \cdot (u')^2, \quad \varepsilon = \frac{c_\mu^{3/4} \cdot k^{3/2}}{d_h} \quad (7)$$

At outflow faces, Neumann boundary conditions with imposed pressure are used.

Non-slip walls enclose the calculation domain. Wall functions are used to model momentum exchange between walls and fluid. Here, the general wall law of Reichardt (Reichardt, 1951) is applied that spans with one correlation the three sublayers of viscous-, buffer- and logarithmic law region ($\kappa=0.415$). The correlation is written for the non-dimensional velocity U^+ :

$$U^+ = \frac{U}{U_\tau} = \frac{1}{\kappa} \cdot \ln(1 + \kappa \cdot y^+) + 7.44 \cdot \left(1 - e^{(-y^+/11)} - \frac{y^+}{11} e^{(-y^+/3)} \right) \quad (8)$$

U_τ and y^+ are friction velocity and non-dimensional wall distance, respectively. Definitions of all non-dimensional quantities can be found in Pope (2000). Local equilibrium between production and dissipation of turbulent kinetic energy is assumed at the first near wall calculation point. The following boundary conditions for k and ε are derived from Reichardt's wall law (eq.(8)). The functions are written in non-dimensional form:

$$k^+ = \frac{k}{U_\tau^2} = 0.07 \cdot y^{+2} \cdot e^{\left(-\frac{y^+}{9}\right)} + \frac{1}{\sqrt{c_\mu}} \left(1 - e^{\left(-\frac{y^+}{20}\right)} \right)^2 \quad (9)$$

$$\varepsilon^+ = \frac{\varepsilon}{\nu U_\tau^4} = \frac{1}{\kappa \cdot (y^{+2} + 15^4)^{\frac{1}{4}}} \quad (10)$$

4.5. Discretization

In TrioCFD, the conservation equations can be discretized on unstructured, tetrahedral grids by using a finite volume based finite element method (Finite Volume Elements, VEF). The discretization is an extension of the classical Crouzeix–Raviart element (Girault and Raviart, 1986), where the main vector unknowns (velocity) and scalar unknowns (temperature, k , ε and concentration) are located in the centre of the faces of an element whereas the pressure is discretized in both the centre and the vertices of the element. This staggered mesh arrangement is P1-non-conforming for velocity and scalars then P0-P1 for the pressure.

4.6. Solution Method

After discretization, a system of non-linear algebraic equations is obtained, whose unknowns are the discrete physical variables. An implicit, mass-conserving time marching scheme is used. Temporal integration of Navier-Stokes equations is done with a fractional steps method (Ferziger and Peric, 2002):

1. A Reynolds averaged, non-divergence free velocity field $\bar{\vec{u}}^*$ is calculated with the linear system solver GMRES. The convection term is linearized. In vector notation this leads for eq.(2) to:

$$\frac{\bar{\vec{u}}^* - \bar{\vec{u}}^n}{\Delta t} = -\frac{1}{\rho} \nabla \bar{p}^n + \nabla \cdot [(\nu + \nu_t) \cdot (\nabla \bar{\vec{u}}^* + \nabla^T \bar{\vec{u}}^*)] - \nabla \cdot (\bar{\vec{u}}^n \bar{\vec{u}}^*) + \vec{F}_m \quad , \quad (11)$$

2. The intermediate velocity field $\bar{\vec{u}}^*$ is then projected by the pressure solver with the conjugated gradient method into a divergence free space by introducing the increment δp :

$$\delta p = p^{n+1} - p^n \quad , \quad \Delta \delta P = \nabla \cdot \bar{\vec{u}}^* \quad , \quad \bar{\vec{u}}^{n+1} = \bar{\vec{u}}^* - \frac{\Delta \delta P}{\Delta t} \quad (12)$$

4.7. Modelling of the core region

An explicit resolution of the reactor core is not possible to date. Thus, simplifications were introduced, which lead to a basic porosity modelling of the core region. In the VVER-1000 core, fuel pins block about 46% of the volume. Hence, a homogeneous volume porosity of 0.54 is introduced in the calculation for the core region.

To take into account both axial and transverse pressure losses in fuel assemblies, friction coefficients are used. They are defined by eq.(13). The coefficients (Table 4-1) are used at CEA to estimate the pressure losses in fuel assemblies of square arrangement; D_h is the hydraulic diameter of a sub-channel and D_e the minimum distance between two fuel rods.

$$C_f = a \cdot Re^{-b} \quad \text{with} \quad Re = \frac{U \cdot D}{\nu} \quad (13)$$

Table 4-1: Parameters for the pressure loss correlation

Direction	a	b	U	D
Axial	0.316	0.25	$ \bar{u}_a $	D_h
Transverse	4.03	0.27	$ \bar{u}_t $	D_e

These pressure losses are implemented in the Navier-Stokes equations (eq.(2)) as source term $F_{m,i}$.

The core power is taken into account in the energy equation (eq.(4)) by the source term F_e . A time and space invariant source term is applied individually for each assembly.

Results of a reference calculation

A reference calculation has been carried out for nominal reactor conditions. Nominal conditions correspond to the following flow and power characteristics of the VVER-1000 reactor:

- Pressure: 160 bar,
- Cold leg inlet temperature: 287 °C,
- Total flowrate: 16912 kg/s,
- Core power: 3000 MW.

The flowrate corresponds to only 96% of the nominal flowrate to account for the bypass from cold to hot legs. The total flow rate is distributed homogeneously among the four loops (4228 kg/s per loop). A velocity that is constant in time and space is imposed at the inflow faces of the four cold legs. In order to assure the same flowrate in each loop, a negative flow rate is therefore imposed at the hot leg outlets of the loops 1, 2 and 3. Only at the outlet of loop 4, a pressure outlet condition is used.

Concerning the spatial distribution of the thermal power within the core, the horizontal power distribution of the CAMIVVER benchmark has been used. The power is assumed constant per assembly and constant in height.

A transient of about 15 s has been simulated. At the end of the transient, temperature, velocity and pressure fields converge to a stabilized solution. The velocity and temperature distribution in a vertical plane, cut through the loops 1 and 3 are shown in Figure 4.3a and Figure 4.3b, respectively. It is visible, that in the upper plenum, near the outlet nozzles, a steady state solution is not achieved. Rather, velocity and temperature oscillate slightly. This is the reason why a steady state solver could not have been used.

Recirculation zones are predicted below the cold leg inlet nozzles in the diffusor region of the downcomer. Such zones with upward flow have been likewise detected numerically in Pre-KONVOI geometry. Nevertheless, an insufficient fine meshing in the diffusor region might be responsible for this result. Further analysis is necessary.

It is also interesting to note that the temperature in the hot leg stratifies; the hot flow from the external core region arrived on the lower section of the hot leg, whereas the colder flow from the centre of the core arrives on the upper part of the hot leg.

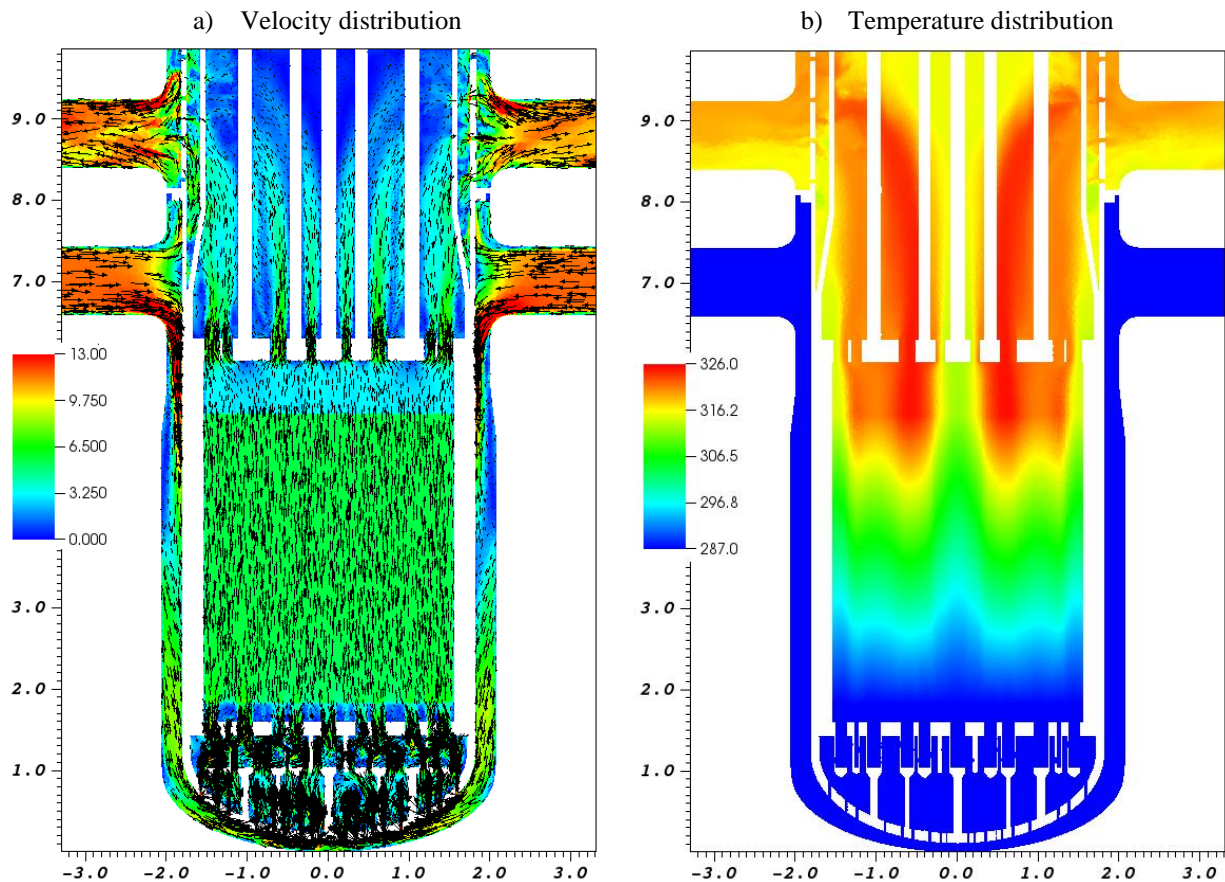
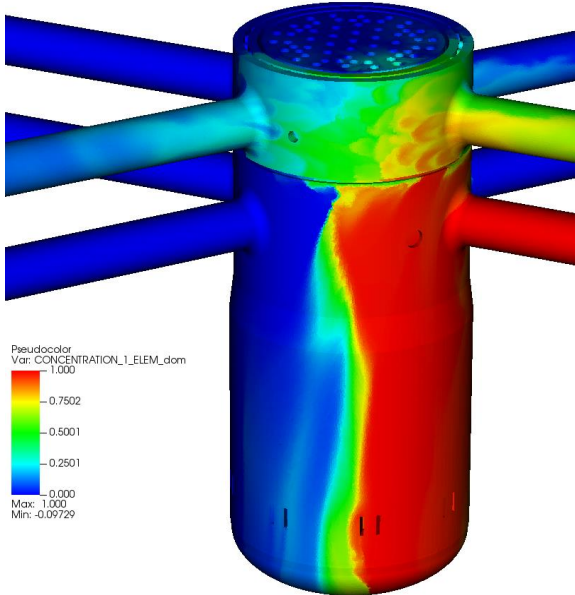


Figure 4.3 : Velocity (a) and temperature (b) in a vertical cut plane for stabilized conditions.

In order to show the mixing between the loops, a passive scalar of concentration “1” is injected into loop 1. The resulting distribution of the scalar in the reactor is shown in Figure 4.4a. The mixing zones in the downcomer is good visible. Likewise, the transfer of flow that comes from loop 1 to loops 2 and 4 is easily detectable. The distribution of the temperature at the upper limit of the active core zone is shown in Figure 4.4b. The hotter and colder zones, which are related to the used horizontal power distribution, are good visible.

a) Visualization by a passive scalar of the flow that comes from loop 1



b) Temperature distribution at the end of the heated zone of the core

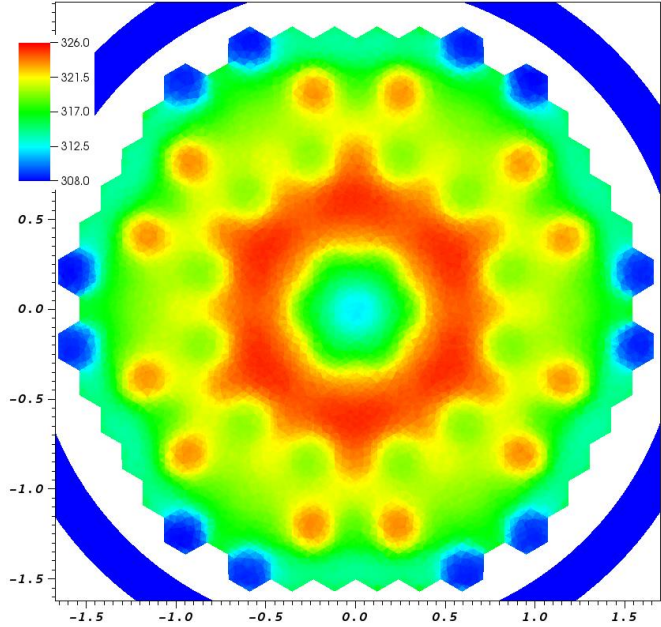


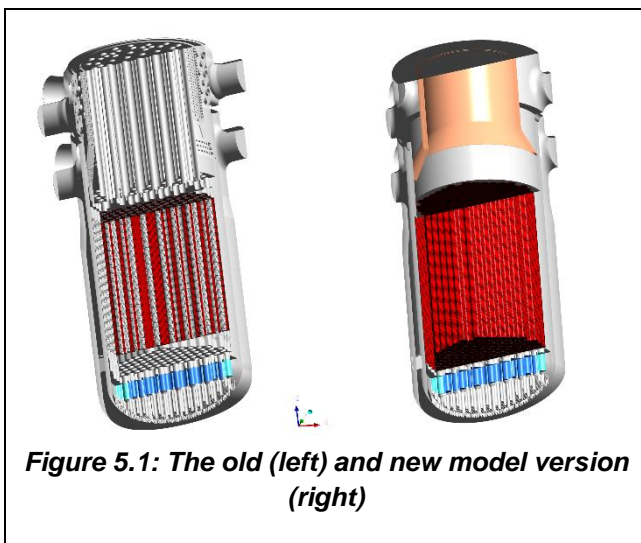
Figure 4.4 : Concentration of a passive scalar (a) and temperature at the end of the active core (b).

5. Description of KIT CFX model

The main problem for the creation of a detailed CFD model for a geometrical high complex technical system like the VVER1000 nuclear pressure vessel is to develop an adequate computational mesh that is able to resolve all relevant flow scales inside the pressure vessel. At a vessel height of about 10m and a diameter larger than 3m, the smallest geometrical relevant scales have 3mm such as the gap width of perforations in the upper part of the core support columns. The coolant reaches locally a maximum speed of nearly 30m/s – while passing through the holes of the elliptical bottom plate - which requires a smallest wall spacing of 0.02mm in order to be close to y^+ values of 100. Fortunately, the Reynolds number is large ($>1e6$), so that values for $y^+ \gg 100$ are acceptable mainly for the computation of pressure losses. For the accurate calculation of heat transfer, the general recommendation is a value of $y^+ \approx 1$, which is impracticable because of limitation of computational resources. For practical reasons, several regions of the pressure vessel are meshed as porous medium: the core, the upper part of the core support columns and nearly the complete part of the upper plenum.

As former participant of a VVER1000 benchmark by OECD an older CFD model from 2009 was activated again and updated to one of the latest ANSYS CFX versions (2020 R2). For meshing, Pointwise for the new versions and Gridgen – a former version of Pointwise software – is used. The new version provides a feature for semi-automatic boundary layer inflation, which was used intensively for the meshes of the new model.

Figure 5.1 shows both CFD model versions. While the old version represents the upper plenum in full detail, the new version represents here an inner perforated wall as porous region. Several differences in detail modelling are visible. The new model does not take into account the upper core plate, which is resolved in the old version. The core is modelled as porous region by individual resolution of all assemblies, while the old version resolves assemblies as subchannels with empty centre volumes equal to the volume of the fuel pins. For all models between the core and the core barrel, a small bypass channel at gap width of about 25 mm is created. The bypass mass flow of about 2.9% is regulated by the introduction of an additional pressure loss coefficient for this channel. Below the core (red region), nozzle connections between each assembly and the core support plate are modelled in the new version, while this volume is considered as empty space in the old version. The core support plate is fixed by support columns against an elliptical bottom plate, which is finally connected with vessel wall structures. The upper part of the core support columns is perforated by



small slots at its outer shells and serves as flow path from the lower plenum into the perforations of the core support plate, see blue and turquoise centre inside Figure 5.1. It is modelled as porous region with adjusted pressure loss coefficients de-rived from former CFD detail simulations. For the support columns in peripheral location, the loss coefficients are higher than for the others because the slot arrangement is different. The loss coefficients applied for the core region, the upper core support columns and for the upper plenum (only for the new model version) are fixed to obtain the design pressure drops at nominal steady state conditions [4]. For a more detailed description of the porous region loss

coefficients see [5] and [6].

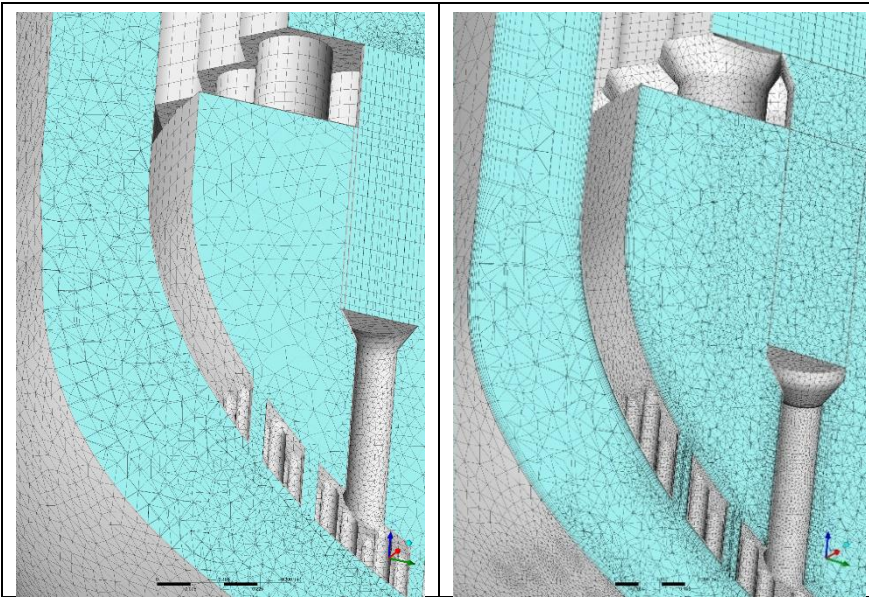


Figure 5.2: coarse mesh (V1) and very fine mesh (V3)

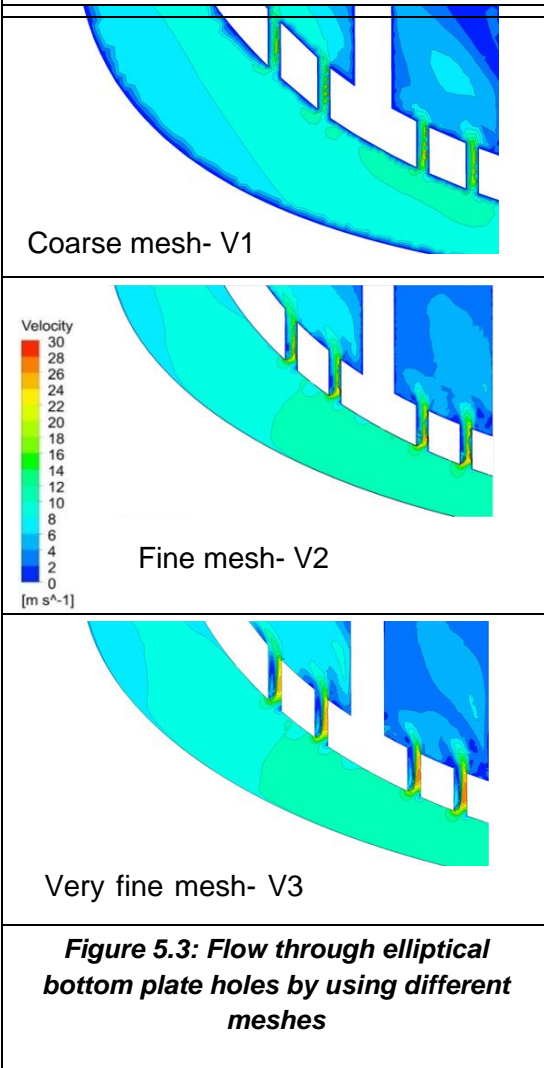


Figure 5.3: Flow through elliptical bottom plate holes by using different meshes

For all model versions unstructured meshing was used with cell scales from 5-50mm for the old version (V1, 23.8 million cells) and 1-40 mm for the new version (V2, 36.2 million cells) with medium spatial resolution and boundary layer inflation from the inlet centres and the downcomer until the entrance holes of the elliptical bottom plate. An additional mesh refinement for the new version model is performed by the extension of boundary inflation through the elliptical bottom plate holes into the

lower plenum (V3, 57.6 million cells). Figure 5.2 shows a part of the mesh in the lower plenum at the elliptical bottom plate which represents in terms of meshing the most crucial part of the pressure vessel. Local mesh refinements at the outer vessel wall below the holes of the elliptical bottom plate were necessary to generate a smooth transition region between the inflation fronts inside the downcomer. The thickness of the wall closest inflation layer varies between 1mm in the downcomer and 0.25mm inside the bottom plate holes.

Figure 5.3 shows the influence of the meshes on the flow patterns inside the elliptical bottom plate holes, where the highest flow velocities and highest wall shear stresses inside the vessel are located. The velocity distributions are calculated for steady state normal operation conditions at a total mass flow of 17.583 tons/s, a temperature of 287°C at the inlets and a pressure of 15.6 MPa. The coarse mesh V1 without boundary layer inflation overestimates the boundary layer thickness in the downcomer and is not able to calculate local flow separation inside the holes. For the fine mesh V2, the boundary layers in the downcomer are better resolved and flow separation in the holes is calculated but obviously with some numerical diffusion and numerical noise.

The best convergence was obtained with the finest mesh V3, where the separation zones are more stable

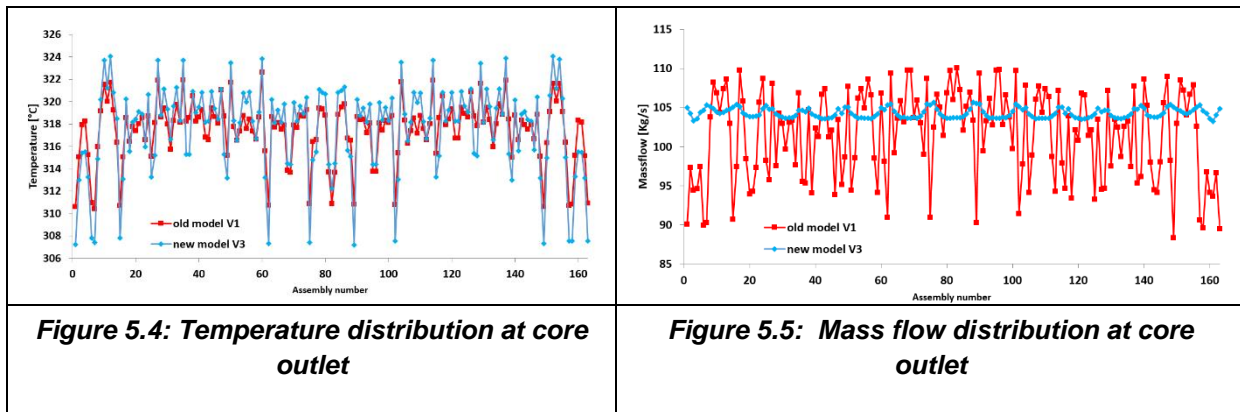
and better resolved by the mesh. As convergence criteria, the normalized RMS residual values mainly for pressure and velocity components and the global balances for momentum and energy equations are used. For all cases RMS values were slightly higher than 10^{-4} ($1.6 \cdot 10^{-4}$ for V3 and

$4 \cdot 10^{-4}$ for V1), while the accuracy for the global balances was $<1\%$ for all cases. Within 200 iterations, convergence for a steady state simulation could be achieved.

All models apply a SST $k-\omega$ turbulence model by Menter [7] with a standard 1st order discretization scheme. All other equations are solved with a high order scheme with 1st order in regions with strong gradients and 2nd order in other regions by Barth and Jespersen [8].

The models include the following simplifications:

No solids were considered because of the low heat capacity of steel compared with coolant and lower mass inventory. Steel has a significant higher thermal conductivity than water, but the energy transport by conduction is negligible against convection. All outer boundaries were assumed as adiabatic because of the large volume-to-surface ratio so that any losses can be neglected. Several design elements were not considered by the mesh such as fuel pins or spacers. In general, the new model versions provide a higher mesh quality, while for the upper plenum the old model is significantly more accurate. First tests have shown that mixing in the upper plenum is calculated as more intensive by the older model and shows significant differences from mixing in a porous media model. The coolant properties were implemented as temperature and pressure dependent by using the IAPWS water data library in ANSYS.



The influence of the mesh on temperature and mass flow distribution at the core outlet is shown in Figure 5.4 and Figure 5.5. For these simulations steady state again normal operation conditions were assumed with a thermal heat release of 3000MW. Assembly averaged power factors and a core averaged axial power distribution were calculated by a standalone Trace/Parcs simulation and taken as input for the CFD models. With the V3 mesh, the mass flow distribution for the assemblies is calculated with a variation range of about $\pm 2\%$ with a local minimum at the central assembly and maximum values at the peripheral assemblies for the assembly layers. The variations calculated by V1 are significantly higher up to $\pm 10\%$ concerning the average value. Local differences between V1 and V3 may reach a level of about 15%. Temperature and mass flow deviations between V1 and V3 are in negative correlation, because the consequence of a lower mass flow is a higher temperature in case of the same heat release. Local differences up to 3°C are calculated which means relative differences of 10% if the average heat up of the coolant of about 30°C is considered as reference temperature. Obviously, the calculated temperatures at the core outlet are less sensitive for meshing.

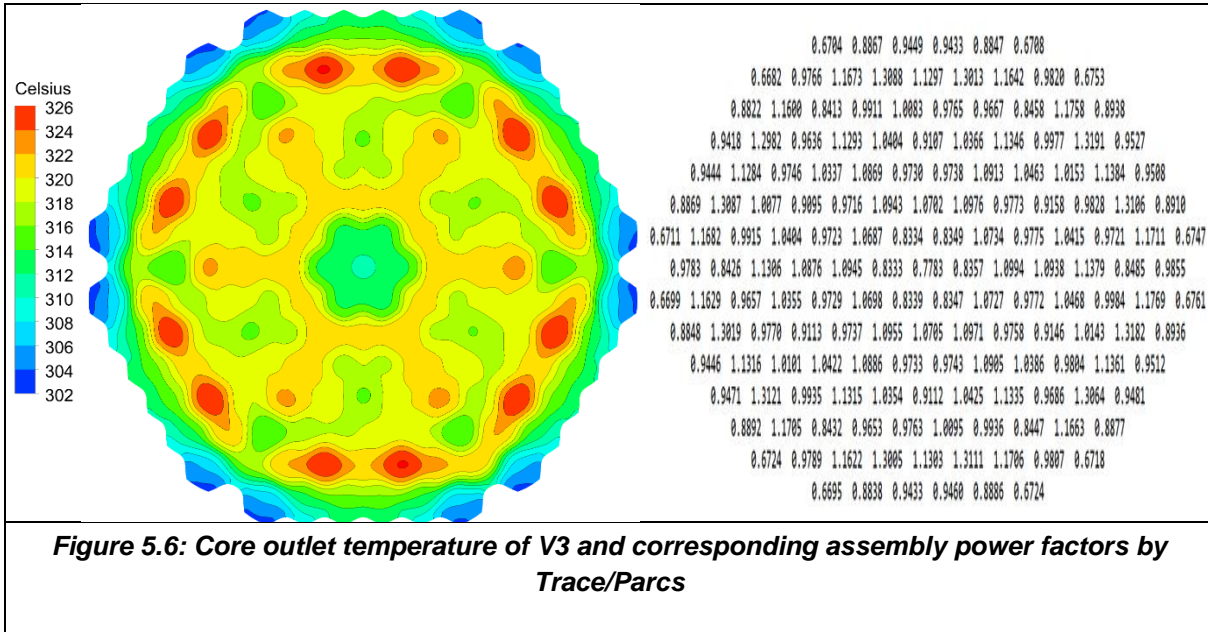


Figure 5.6: Core outlet temperature of V3 and corresponding assembly power factors by Trace/Parcs

In Figure 5.6 the core outlet temperature distribution from model V3 and the corresponding assembly power factors are shown. The lowest assembly temperatures are located in radial peripheral positions, where the assemblies with the lowest power factors are found and a mixing with colder bypass coolant takes place. In general, the temperature patterns correlate with the power factor distribution. The hot spot temperatures are located at assemblies with power factors larger than 1.3. The heat and mass exchange between neighbouring assemblies is reducing the temperature differences, but the signature of the power factor distribution is clearly visible at the core outlet.

The numerical accuracy of the new model versions V2 and V3 could be significantly improved against the older V1 version because of advances in meshing technics not implemented in meshing tools more than a decade ago. By using boundary layer inflation, y^+ values inside the holes of the elliptical bottom plate could be reduced from 30000 in V1 below 1000 for the V3 version. Concerning the computational costs for steady state simulations, the V3 model consumes about 1 day (by 30 CPU's). For transient cases, the V2 model will be used as compromise.

6. Description of FRAMATOME STAR-CCM+ model

The model is built with STAR-CCM+ v.2021.1, most of the data used to create it was found in the document in reference [2].

6.1. Geometry

The geometry represented in the model is of the primary vessel. It spans from the cold legs, through the downcomer, the core and the upper plenum to the hot legs. The domain used in the calculation is shown on the Figure 6.1.

The core geometry is simplified (in orange on the Figure 6.1): each assembly is modelled by a porous medium, thus the spacing grids and the fuel rods are not explicitly represented. Similarly, the basket enclosing the core, the plates in the upper plenum, the shielding block tube and the grid in the vessel before the hot legs are treated as porous media (in grey on the Figure 6.1). The holes in the support columns are not explicitly represented either, a head loss coefficient is used to model their influence on the flow.

There is no circulation in the spacer ring between the cold legs and the hot legs, the whole flow must go through the downcomer.

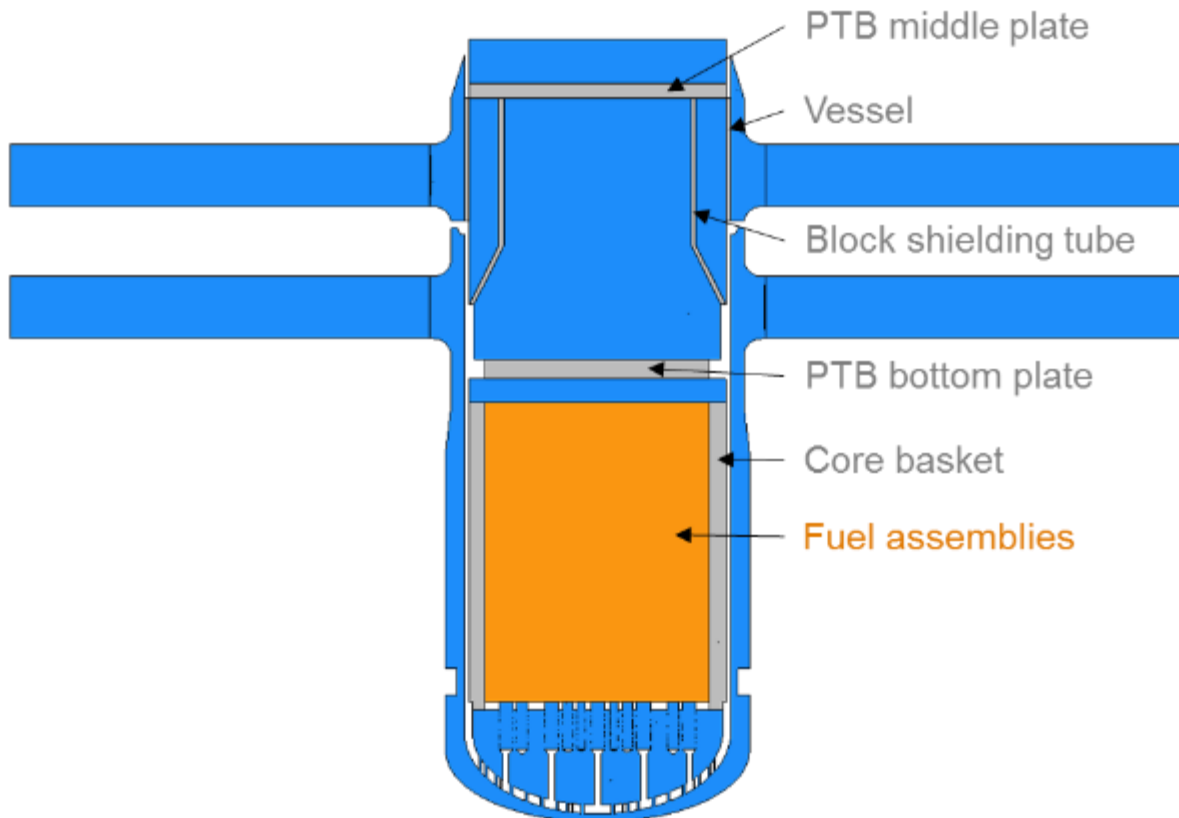


Figure 6.1: Overview of the geometry

6.2. Meshing

The mesh is made of polyhedral cells and contains approximately 48 million cells. Boundary layer refinements are made to keep y^+ values under 300 in most of the domain. An overview of the mesh is given on Figure 6.2.

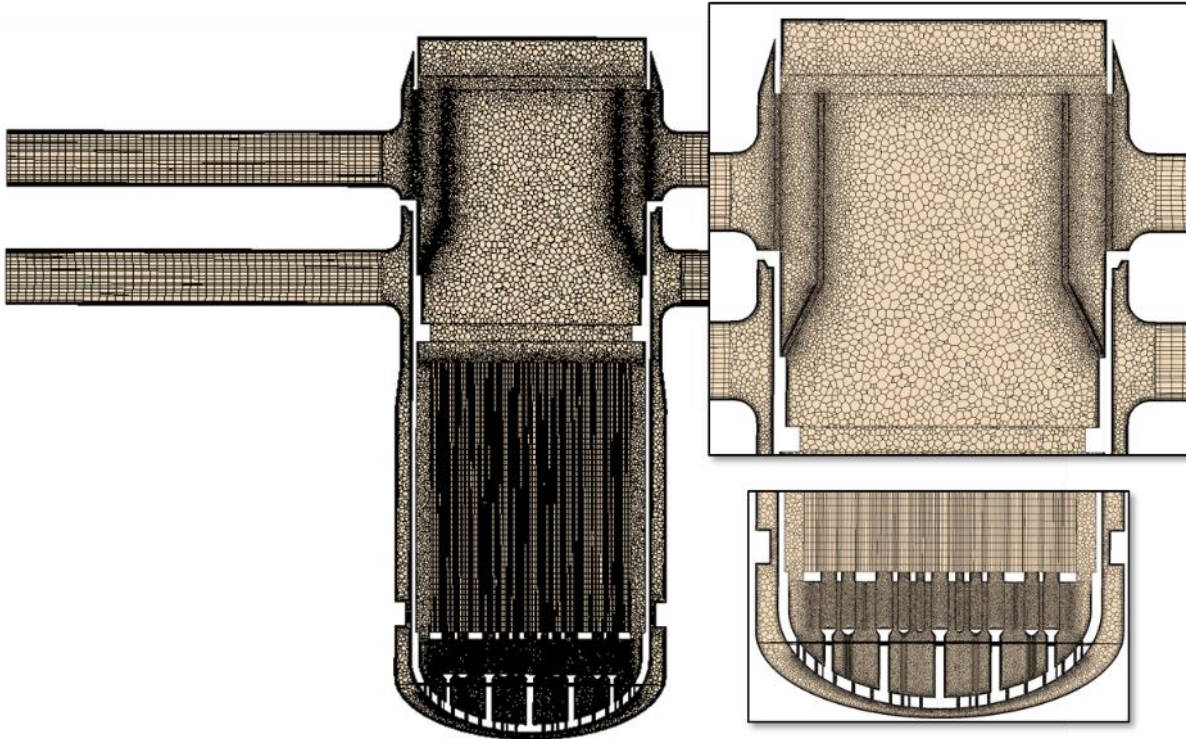


Figure 6.2: Mesh overview

6.3. Boundary conditions

A mass flow inlet condition of 17612 kg/s is set on the cold legs (4403 kg/s each) with a fluid temperature of 287 °C.

On the hot legs, a pressure outlet condition is applied.

6.4. Head loss coefficients

Head loss coefficients are applied at the following locations to regulate either the mass flow or the head variation:

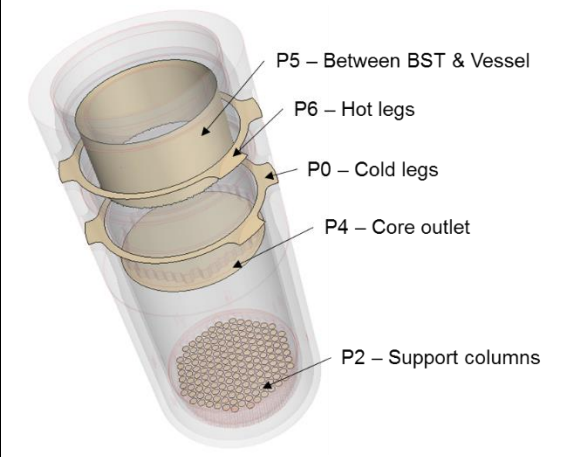
- In the core basket to control the by-pass of the core;
- In the support columns to set the head loss through the orifices;
- In the core to account for the grids (axially) and the rod bundles (horizontally);
- Through the base plate of the block shielding tube;
- Through the block shielding tube;
- Through the vessel before the hot legs.

The mass flow by-passing the core is 2.9% of the total mass flow delivered by the pumps.

The head loss coefficients are adjusted to fit the following Table 6-1:

Table 6-1: Head losses in the vessel

Zone	ΔP [MPa]
P0 - P2	0.1971
P2 - P4	0.1422
P4 - P5	0.0284
P4 - P6	0.0363
P0 - P6	0.376



The pressures are measured as follows:

- P0 is in a horizontal section of the downcomer, the altitude corresponds to the centre of the cold legs;
- P2 is in a horizontal section of the support columns;
- P4 is above the core, before the bottom plate of the BST;
- P5 is a radial section of the upper plenum between the BST and the vessel;
- P6 is in a horizontal section whose altitude matches the centre of the hot legs.

6.5. Power source

The core releases a power of 3000 MW, which is represented through a volumetric heat source in the fuel assemblies. The radial distribution of power between the assemblies is detailed in the reference [2] and illustrated on Figure 6.3. The axial distribution of power in the assemblies is not represented in the model, the source is considered uniform over the length of the reactive portion of the rods.

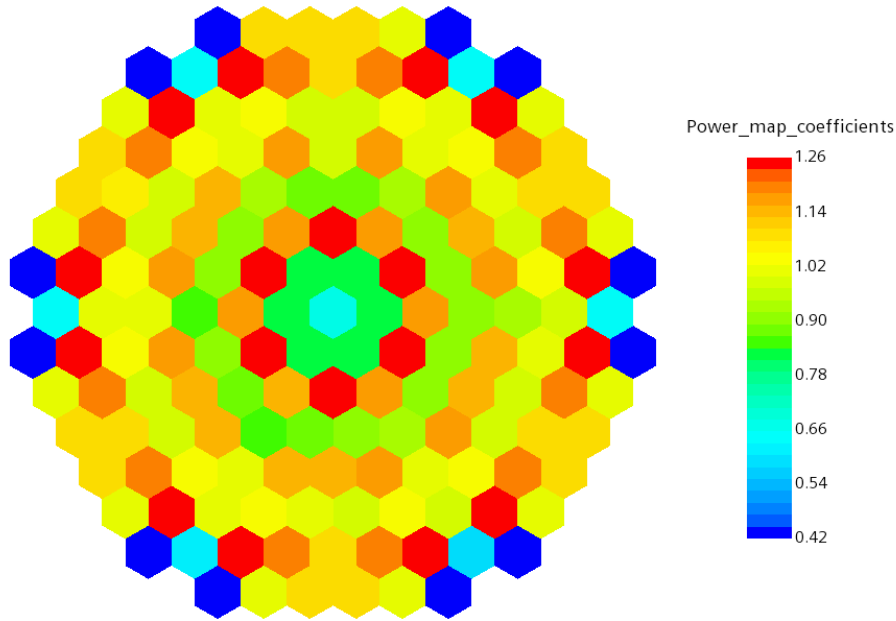


Figure 6.3: Radial distribution of power in the core

6.6. Numerical parameters

The fluid solver used for the calculation is a segregated steady RANS model, with 2nd order spatial schemes. The turbulence model used is K-epsilon Realizable Two-Layer. The thermal solver is a segregated one with 2nd order schemes too.

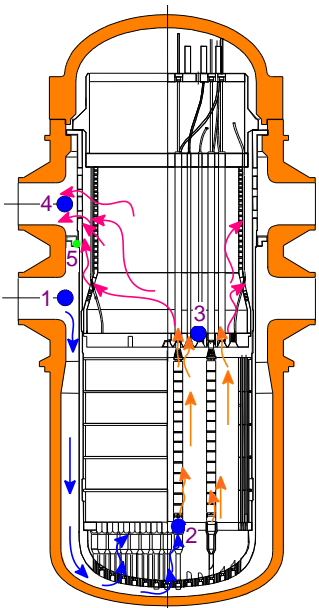
The following properties of water are used, with T_c the temperature in °C :

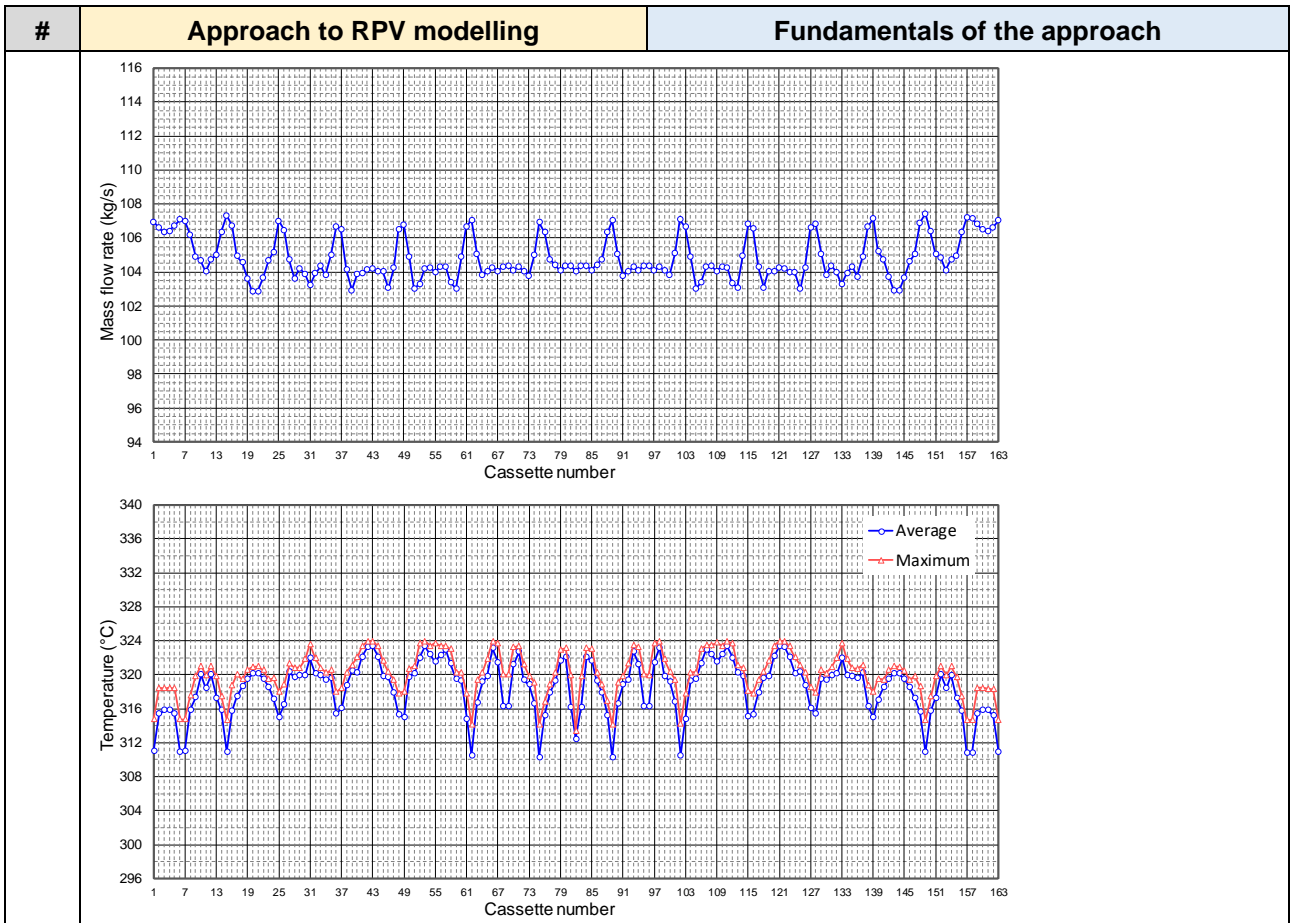
Density [kg/m³]	$3573.393 - 28.26898 * T_c + 0.1004155 * T_c^2 - 1.260181 \times 10^{-4} * T_c^3$
Specific heat [J/(K.kg)]	$1212344.0 - 17044.71 * T_c + 90.04235 * T_c^2 - 0.2111469 * T_c^3 + 1.856398 \times 10^{-4} * T_c^4$
Thermal conductivity [W/(K.m)]	$0.329343 + 0.00344348 * T_c - 8.8837710^{-6} * T_c^2$
Dynamic viscosity [Pa.s]	$6.654779 \times 10^{-4} - 5.107215 \times 10^{-6} * T_c + 1.611641 \times 10^{-8} * T_c^2 - 1.83385 \times 10^{-11} * T_c^3$

7. Description of ENERGORISK Fluent model

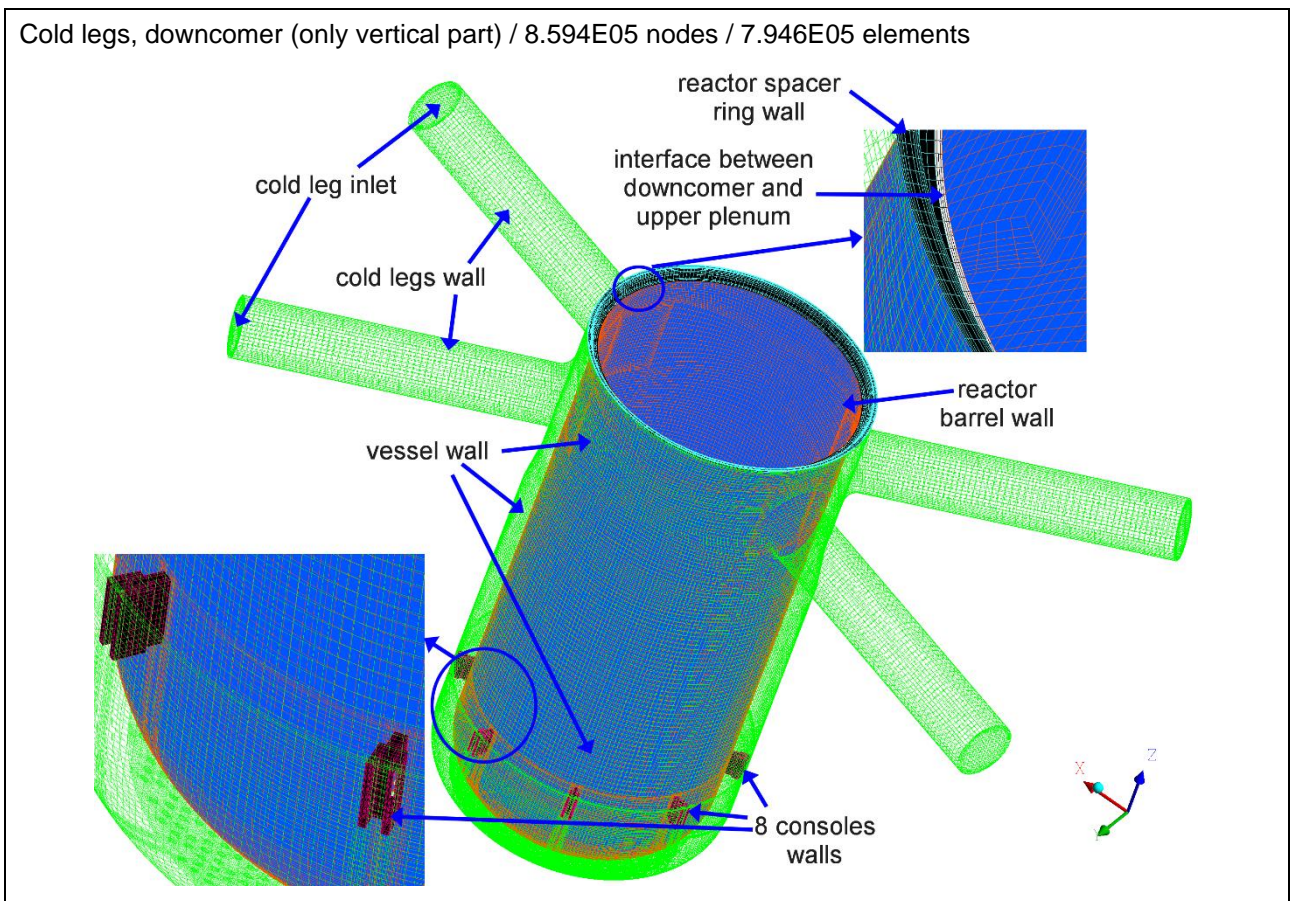
7.1. General approach to RPV modelling

#	Approach to RPV modelling	Fundamentals of the approach
1. Basic modelling simplifications		
1.1	Solid volumes of the reactor vessel and in-vessel equipment are not considered / adiabatic boundary conditions on surfaces (contact “fluid-solid”)	The phenomenology of the studied processes (RPV mixing problem) is automodal with respect to the possible influence of the heat energy of solid volumes – processes with sharp cooldown or heatup of the reactor as a whole, with the possibility of a heat transfer crisis, or processes in long-term (dozens of hours) cooldown/heatup of the reactor system are not considered. RPV mixing problem excluding solids practically does not lose physical essence and correctness and, at the same time, has much less loading on computational resources; this approach is widely used in international experience of the RPV mixing problem analysis with using of the CFD methods
1.2	The core is modelled in a simplified manner using a porous media approach. For each fuel cassette provided individual cell zone with “porous zone” condition; fuel cassettes cross-flow are provided by internal interior interface	Simplified modelling involves by technical plan document. Reactor core porous media approach is widely used in international experience
1.3	Supporting columns perforations (lower plenum), shielding tubes block perforations (upper plenum), reactor barrel perforations (upper plenum) and cross-flow between downcomer and upper plenum (around reactor spacer ring) are modelled in a simplified manner by porous jump approach at fluid-fluid interfaces	Simplified modelling involves by technical plan document. Porous jump model provides sufficient accuracy and correctness of the fluid flow distribution (takes into account the fluid flow area and hydraulic resistance of the space area, which is replaced by a flat porous jump interface) in case of impossibility/complexity of modelling a real geometrical profile
1.4	The buoyancy effects were neglected	High Reynolds number of flow and lack of conditions for the formation of the contour of natural circulation
2. Main aspects and detail of modelling		
2.1	<p>Calculated mesh concept:</p> <ul style="list-style-type: none"> - the total RPV-model volume is divided into several parts, for which an exclusively structured mesh is formed based on hexahedral elements type; - these mesh parts are connected using fluid-fluid type of interfaces; - core mesh model involves the allocation of 163 volumes of individual cassettes connected by an interior interface and forming 163 cell zones; all other mesh volumes are formed one fluid cell zone 	<ul style="list-style-type: none"> - a structured qualitative mesh ensures stable convergence, correctness of the calculated results and acceptable problem/CPU time with the available underpowered computer resources; - the increase in CPU load due to the relatively large number of interfaces is offset by the efficiency of the structured mesh; - mesh convergence studies are considered (coarse, medium and fine meshes) and represent the initial stage of model validation; the medium mesh (17.28E06 nodes) chosen as the most optimal
2.2	<p>Turbulence modelling:</p> <ul style="list-style-type: none"> - RANS approach is considered; 	<ul style="list-style-type: none"> - this turbulence model brings together opportunities k-w turbulence models family (correctness of

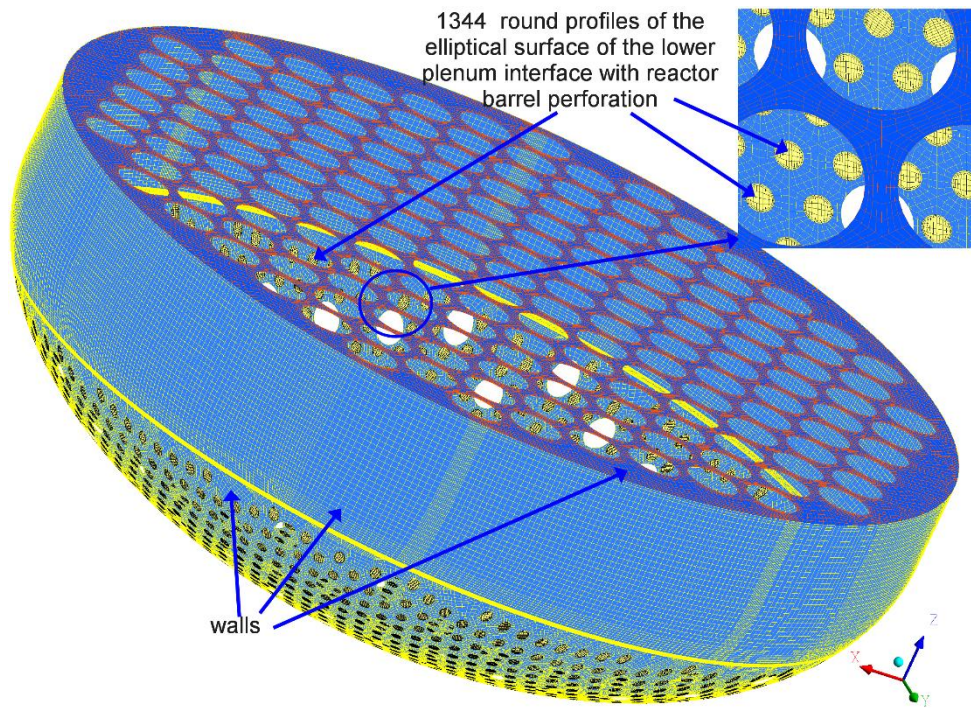
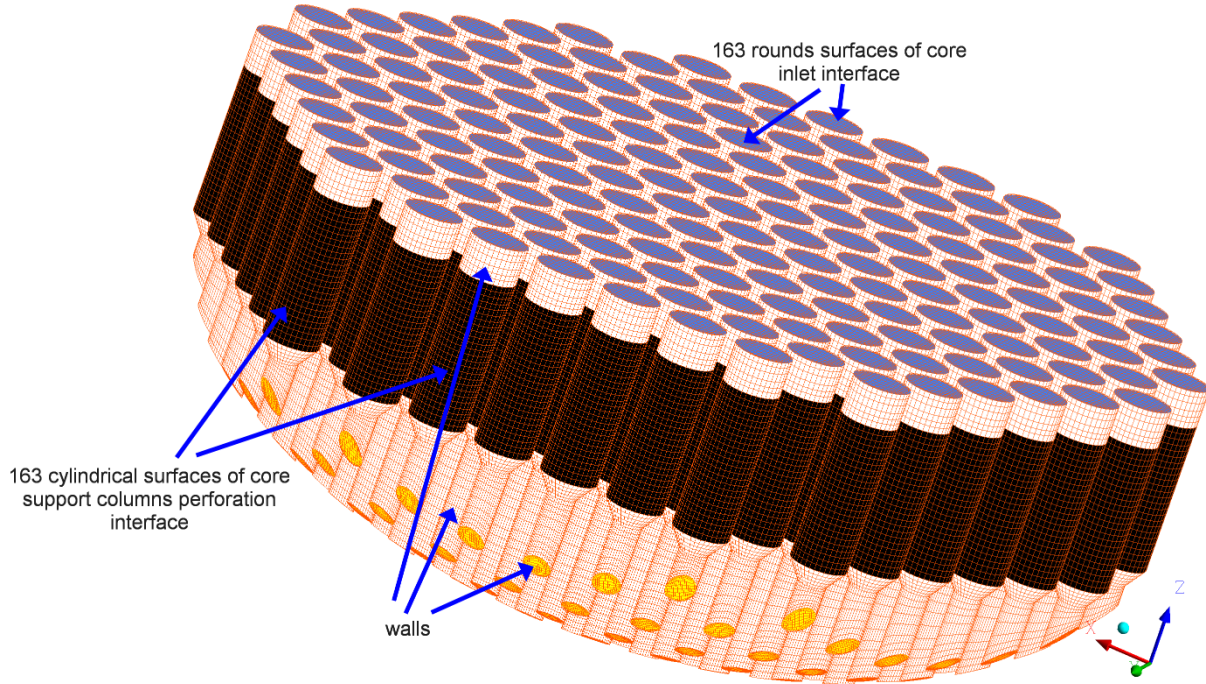
#	Approach to RPV modelling	Fundamentals of the approach																																
	<ul style="list-style-type: none"> - the SST k-ω turbulence model is selected; - the scalable wall treatment is selected 	numerical analysis at low Reynolds numbers) and k- ϵ turbulence models family (correctness of numerical analysis at high Reynolds numbers, taking into account the vorticity and mixing of flows)																																
2.3	<p>Boundary conditions:</p> <ul style="list-style-type: none"> - inlet: the fully formed velocity profile is considered which provides the necessary mass flow; T=cold legs temperature; - outlet: the pressure at the outlet from the reactor and the backflow temperature equal to the average temperature at hot legs outlet are considered; - walls: adiabatic thermal conditions; smooth walls 	<ul style="list-style-type: none"> - for all considered computational analyses, a similar topology of mass and thermal boundary conditions is assumed; - the details of the boundary conditions are selected based on modelling experience and recommendations for the CFD-code under consideration 																																
2.4	<p>Core model:</p> <ul style="list-style-type: none"> - porous media approach involves modelling of viscous and inertial losses; the main axial direction and the direction of transverse losses (loss multiplier=10÷50) are considered; - heat energy source are modelled individually for all cassettes; cassette energy source is formed in the form of an axial profile based on axial non-uniformity of energy release and uneven energy release coefficients 	<ul style="list-style-type: none"> - the choice of parameters of the cassettes porous medium is made iteratively with subsequent adjustment to the required or design parameters of the reactor; - the cassettes heat energy source profiles are adjusted using multiplier factors to provide the required total core power 																																
2.5	<p>RPV model adjustment:</p> <p>- adjustment of the pressure drop in the sections of the reactor and leakage from downcomer to upper plenum is implemented by simulating additional inertial losses at some interfaces with porous-jump model</p>	 <table border="1"> <thead> <tr> <th>Reactor element / section</th> <th>Design value</th> <th>Calculated value</th> <th>Absolute relative deviation (%)</th> </tr> </thead> <tbody> <tr> <td colspan="4" style="text-align: center;">Pressure difference (MPa)</td> </tr> <tr> <td>Reactor inlet chamber (section 1-2)</td> <td>0.201</td> <td>0.1990</td> <td>0.995</td> </tr> <tr> <td>Reactor core (section 2-3)</td> <td>0.142±0.025</td> <td>0.1424</td> <td>0.282</td> </tr> <tr> <td>Reactor outlet chamber (section 3-4)</td> <td>0.037</td> <td>0.0369</td> <td>0.270</td> </tr> <tr> <td>Reactor without inlet and outlet nozzles</td> <td>0.380±0.06</td> <td>0.3783</td> <td>0.447</td> </tr> <tr> <td colspan="4" style="text-align: center;">Crossflow between downcomer and upper plenum (percent of the total reactor mass flow rate)</td> </tr> <tr> <td>Gap between reactor spacer ring and reactor barrel (point-5)</td> <td>0.10</td> <td>0.0975</td> <td>2.50</td> </tr> </tbody> </table>	Reactor element / section	Design value	Calculated value	Absolute relative deviation (%)	Pressure difference (MPa)				Reactor inlet chamber (section 1-2)	0.201	0.1990	0.995	Reactor core (section 2-3)	0.142±0.025	0.1424	0.282	Reactor outlet chamber (section 3-4)	0.037	0.0369	0.270	Reactor without inlet and outlet nozzles	0.380±0.06	0.3783	0.447	Crossflow between downcomer and upper plenum (percent of the total reactor mass flow rate)				Gap between reactor spacer ring and reactor barrel (point-5)	0.10	0.0975	2.50
Reactor element / section	Design value	Calculated value	Absolute relative deviation (%)																															
Pressure difference (MPa)																																		
Reactor inlet chamber (section 1-2)	0.201	0.1990	0.995																															
Reactor core (section 2-3)	0.142±0.025	0.1424	0.282																															
Reactor outlet chamber (section 3-4)	0.037	0.0369	0.270																															
Reactor without inlet and outlet nozzles	0.380±0.06	0.3783	0.447																															
Crossflow between downcomer and upper plenum (percent of the total reactor mass flow rate)																																		
Gap between reactor spacer ring and reactor barrel (point-5)	0.10	0.0975	2.50																															
2.6	Core outlet flow distribution parameters (nominal operating mode):																																	



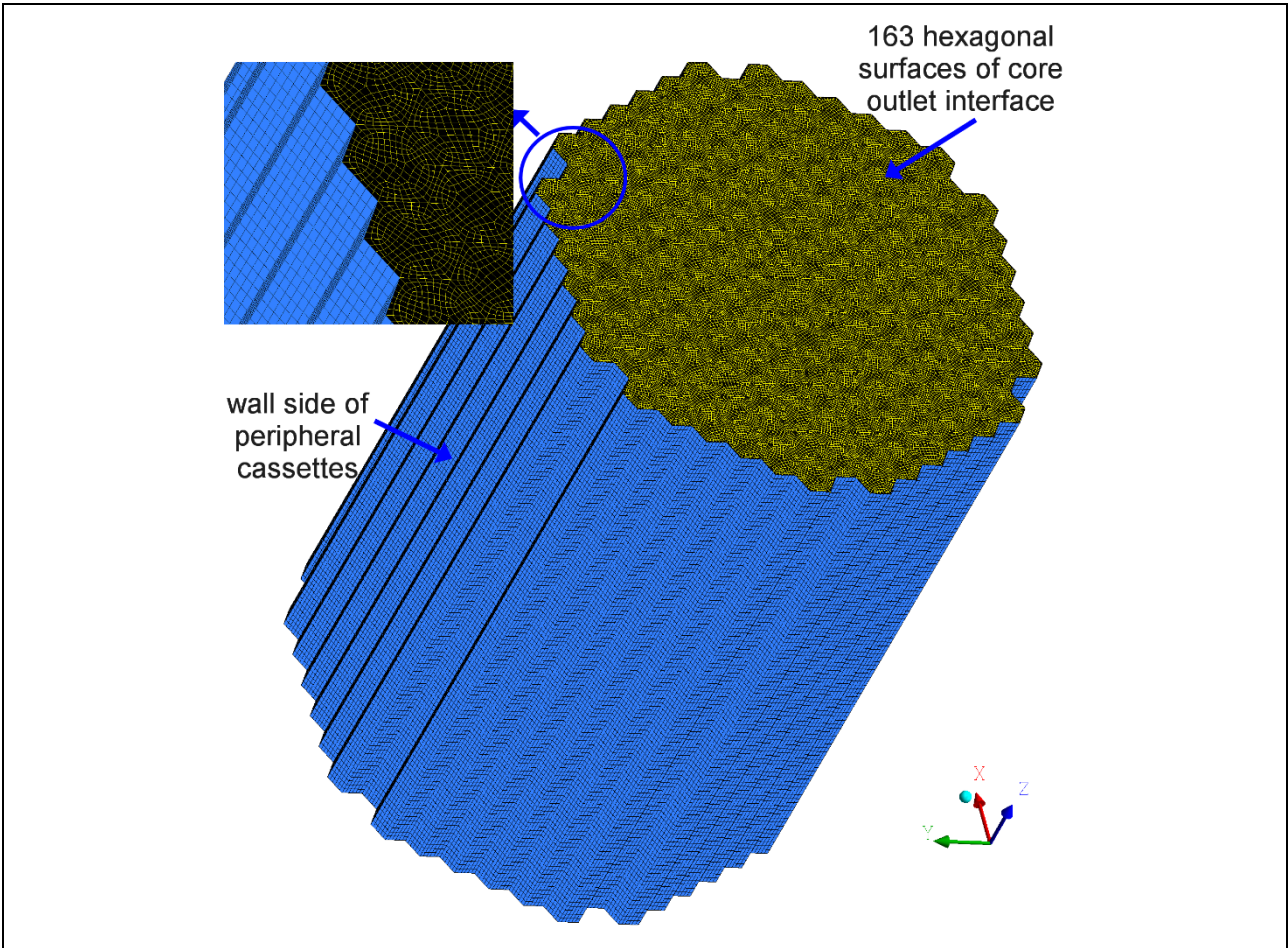
7.2. Geometry and mesh model



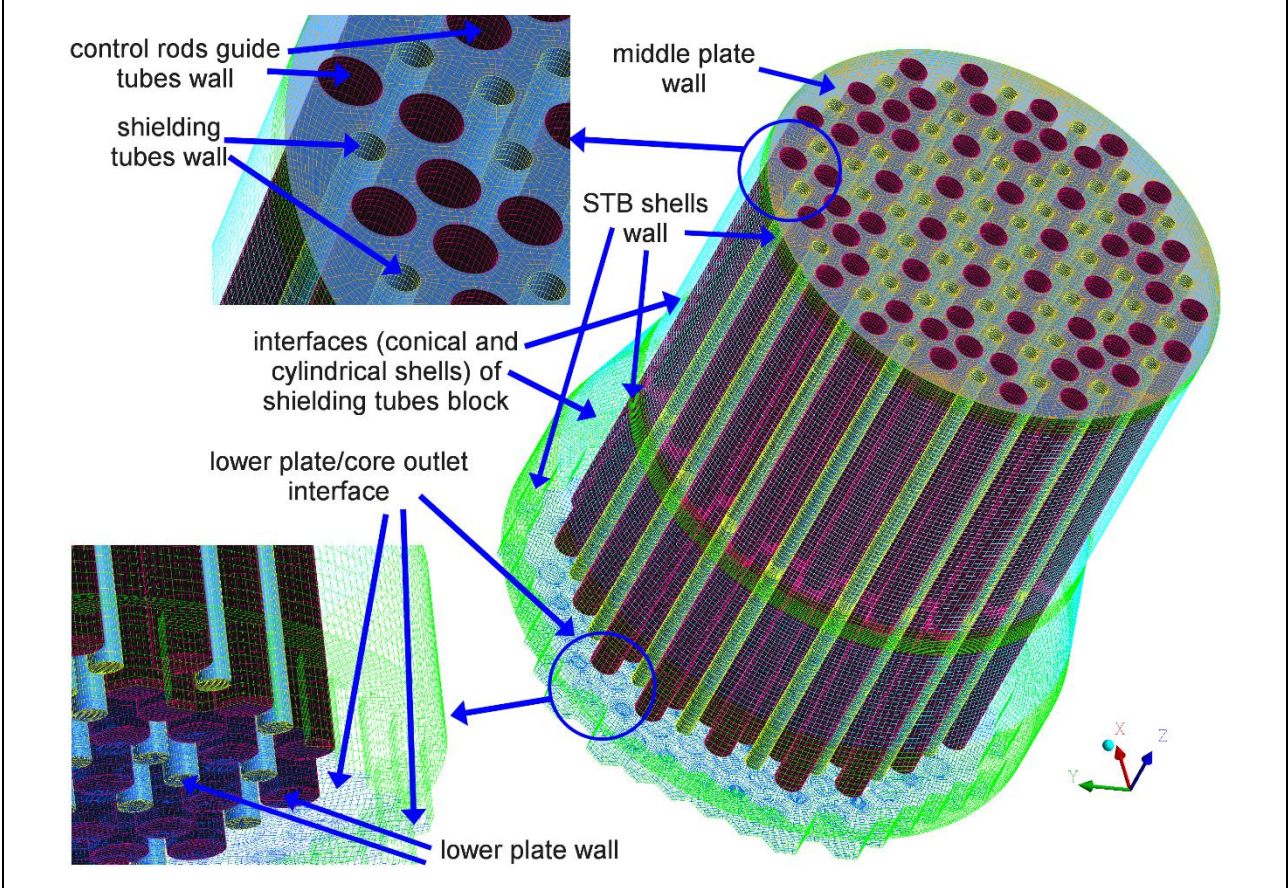
Lower plenum (including space of reactor vessel elliptical bottom) / 9.647E06 nodes / 8.748E06 elements



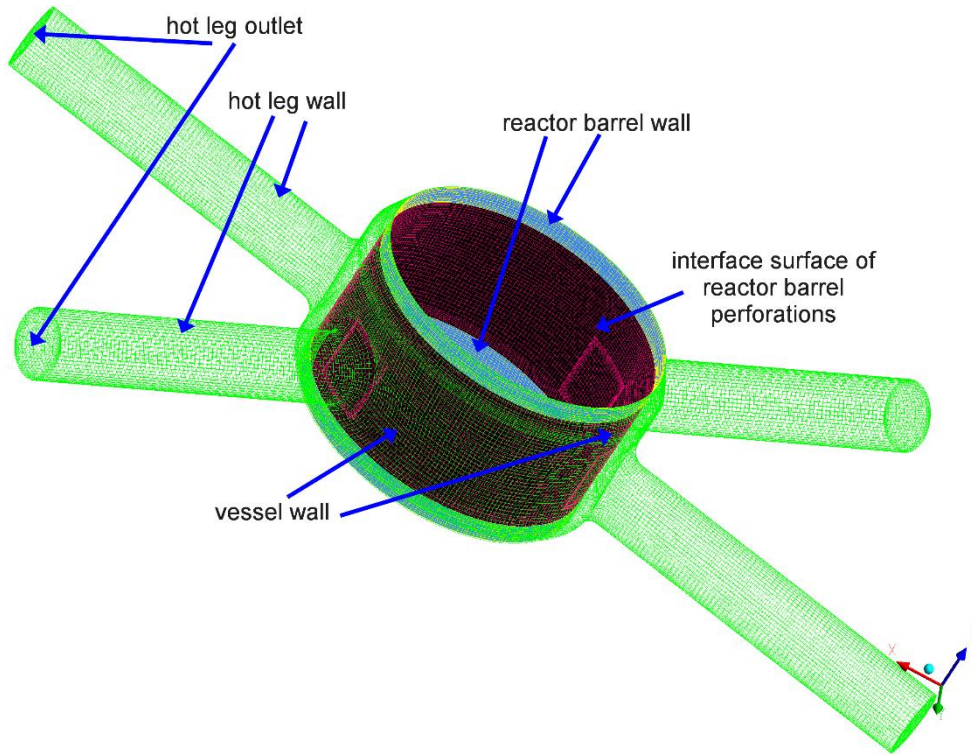
Reactor core / 3.448E06 nodes / 3.076E06 elements



Upper plenum / 2.915E06 nodes / 2.575E06 elements



Hot legs and hot legs collection chamber / 4.154E05 nodes / 3.868E05 elements



8. Nominal full-power steady-state results

8.1. Fuel Assemblies numbering

A common assemblies numbering is used for results comparisons. This numbering is illustrated on Figure 8.1.

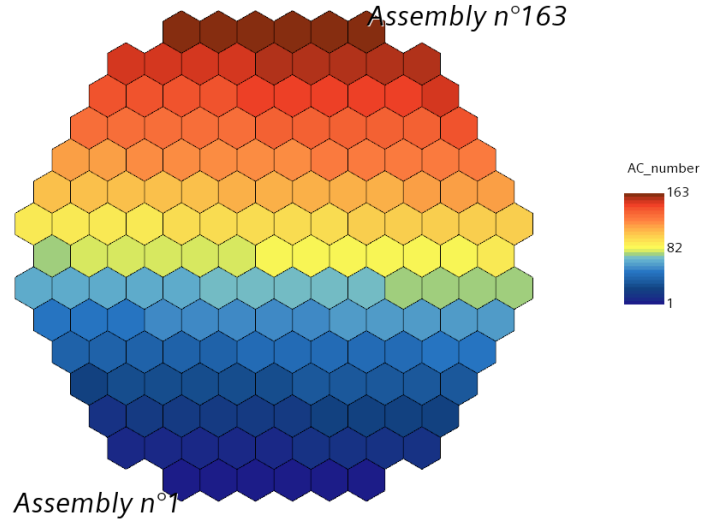


Figure 8.1: illustration of assembly numbering

8.2. Fuel power profile

The fuel power map is given on Figure 8.2.

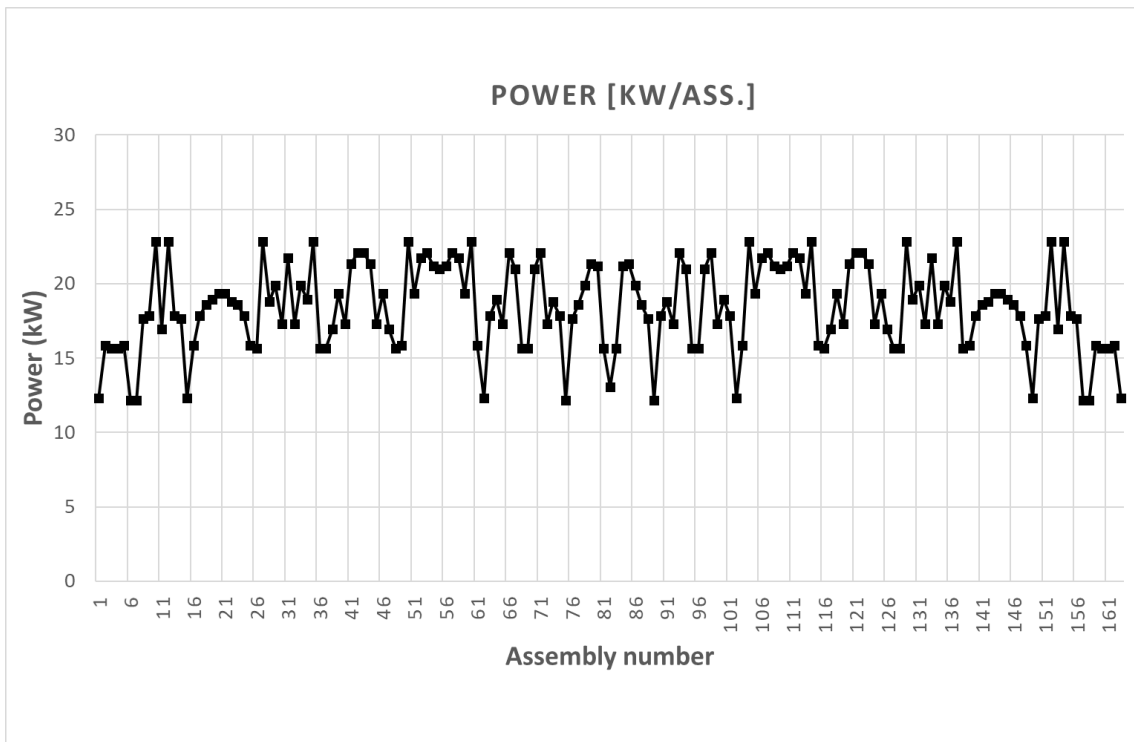


Figure 8.2: fuel power map

8.3. Outlet massflow profile

The outlet massflow profile is given on Figure 8.3. Possible crossflows occurring inside the core between fuel assemblies lead to homogeneous outlet flowrates. Indeed, the difference between minimum and maximum assemblies' flowrate is always below 7 kg/s.

Figure 8.3 shows a good consistency between participants' results, which mainly relies on the fact that all participants' use the same total flowrates.

Assemblies located at the periphery of the core are identified on Figure 8.3 with dark triangle marks below. It underlines that significant differences are observed between participants' results on these assemblies. This has to be carefully considered for the following stages of CAMIVVER workpackage 6.

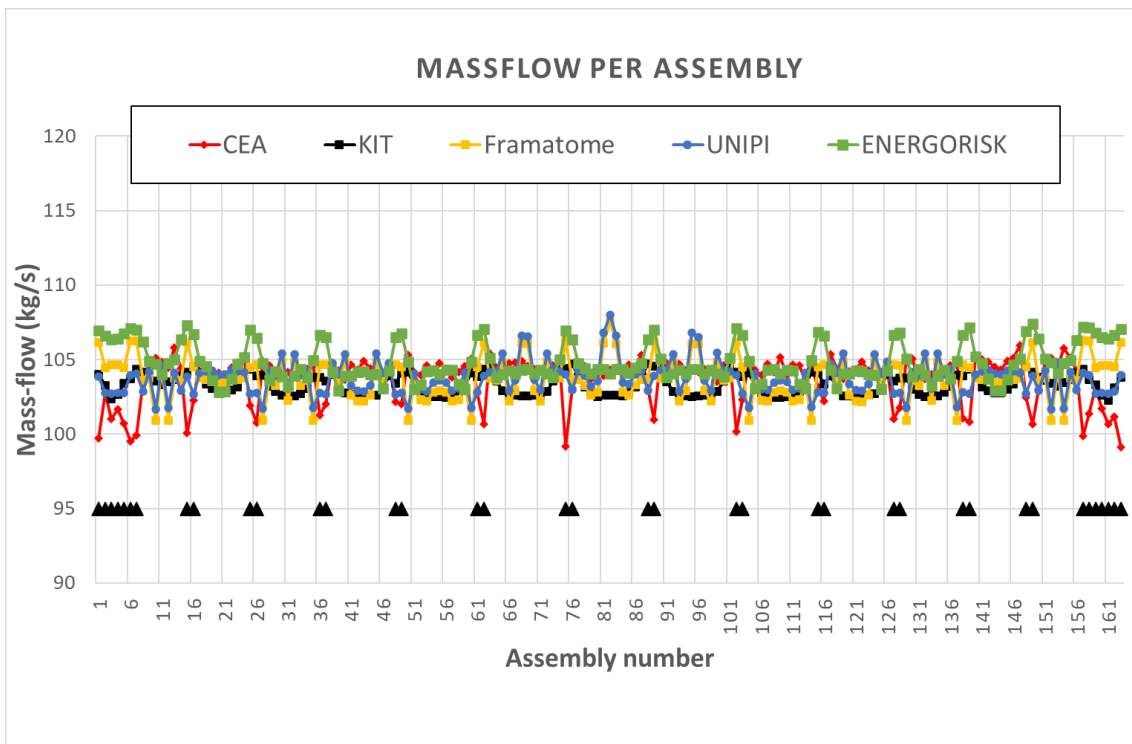


Figure 8.3: assemblies-outlet massflow map
(assemblies located at the periphery of the core are identified with a dark mark below)

8.4. Outlet temperature profile

The mean outlet temperature for each assembly is given on Figure 8.4. These temperatures mainly depend on:

- the radial power map, which is common input data detailed in §8.2,
- the flowrate distribution, which has proved to be consistent among participants within §8.3.

Then, the outlet temperature profile also proves to be consistent among participants. Figure 8.5 illustrates for each assembly the difference between participants' results and the average temperature among participants. This deviation always remains in the range [-3; +3 °C], and almost in the range [-2; +2 °C].

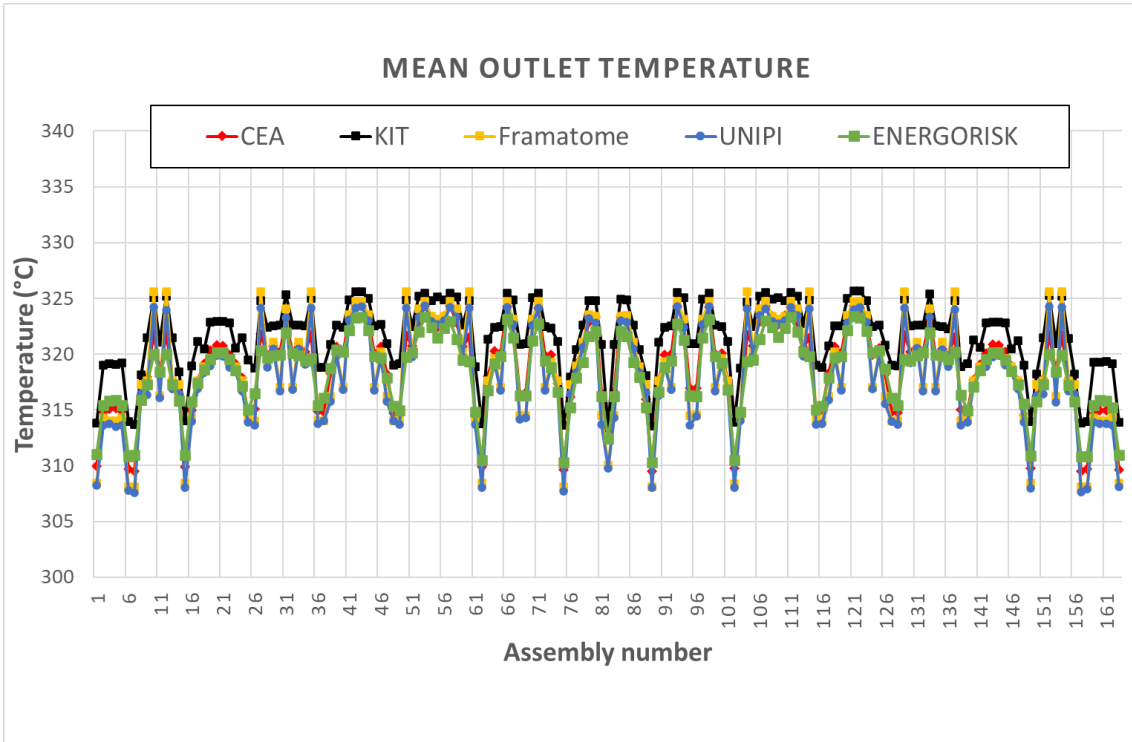


Figure 8.4: outlet temperature map

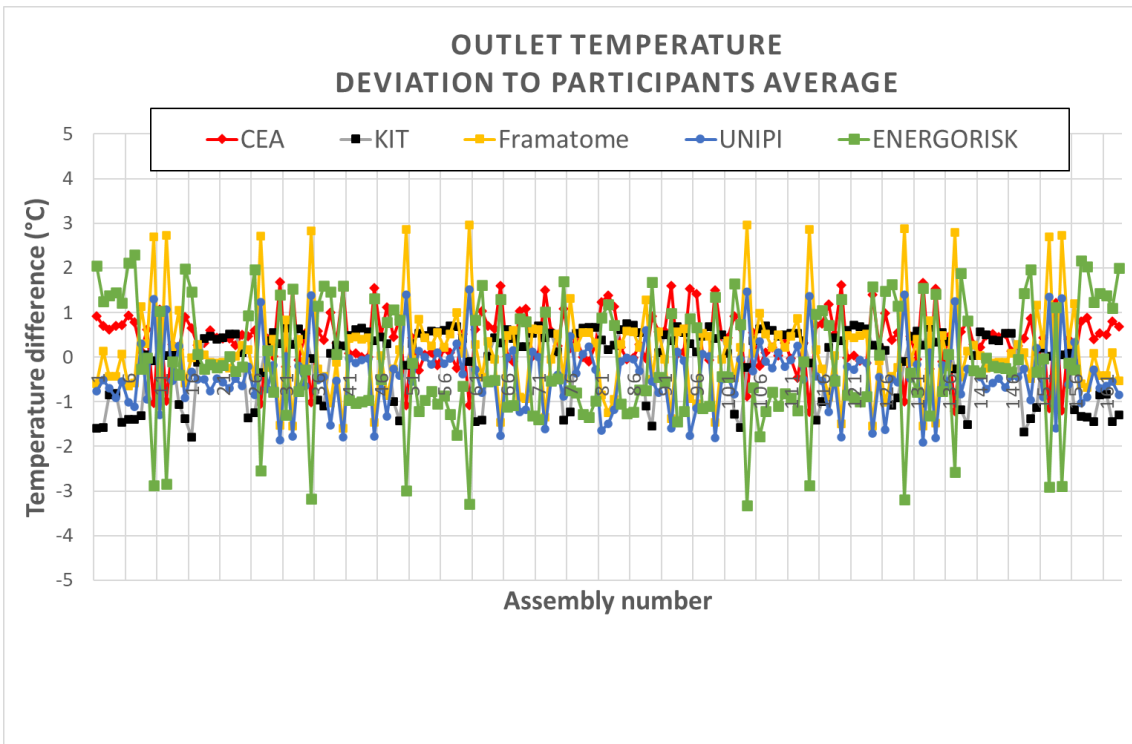


Figure 8.5: outlet temperature: deviation to participants average

9. Conclusion

In the frame of task 6.1 of WP6, participants have developed CFD models of VVER-1000 primary vessel. These models are based on the same CAD model, but have then been developed independently:

- By several participants: KIT, FRAMATOME, CEA, UNIPI, ENERGORISK. Each participants applying his own methodology for meshing, set-up and post-processing.
- Using various CFD tools; CFX, FLUENT, STAR-CCM+, TRIO-CFD

These models have been successfully used to simulate a full-load steady-state operation of VVER-1000. Results obtained have proved to be consistent in such situation.

CFD models are now to be used within task 6.2 dedicated to Kozloduy-6 mixing experiment exercise.

REFERENCES

- [1] Grant agreement, NUMBER 945081 – CAMIVVER.
- [2] CAMIVVER deliverable 3.1
Hashymov Artur, Oleksandr Sevbo (Energorisk), “A comprehensive review of the available VVER data for verification and validation of neutronics and thermal-hydraulics codes”
<http://camivver-h2020.eu/src/assets/doc/D3-1.pdf>
- [3] CAMIVVER deliverable 3.2
Antoaneta Stefanova, Neli Zaharieva, Petia Vryashkova, and Pavlin Groudev (INRNE),
“The CAMIVVER Definition report with specification for NPP with VVER 1000 reactor with respect to selected transients”.
- [4] N.Kolev et. al., 2004 .VVER-1000 coolant transient benchmark (V1000CT), Vol.2, p.21, OECD Nuclear Energy Agency.
- [5] Böttcher, M., 2008. Detailed CFX-5 study of the coolant mixing within the reactor pressure vessel of a VVER-1000 reactor during a non-symmetrical heat-up test. Nuclear Engineering and Design 238, 445–452.
- [6] Böttcher, M., Krüßmann, R., 2010. Primary loop study of a VVER-1000 reactor with special focus on coolant mixing. Nuclear Engineering and Design 240, 2244–2253.
- [7] Menter, F. R., 1993. [*Zonal Two Equation k/omega. Turbulence Models for Aerodynamic Flows*](#). AIAA Journal, 1993–2906.
- [8] Barth, T.J., Jespersen, D.C., 1989. The Design and Application of Upwind Schemes in Unstructured Meshes. AIAA Journal, Paper 89-0366.